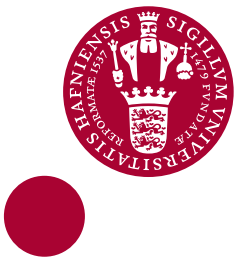

Activation of the ATR kinase by the RPA-binding protein ETAA1

Haahr, Peter; Hoffmann, Saskia; Tollenaere, Maxim A X; Ho, Teresa; Toledo Lazaro, Luis Ignacio; Mann, Matthias; Bekker-Jensen, Simon; Räschle, Markus; Mailand, Niels

Published in:
Nature Cell Biology

DOI:
10.1038/ncb3422

Publication date:
2016

Document version
Peer reviewed version

Activation of the ATR kinase by the RPA-binding protein ETAA1

Peter Haahr[1], Saskia Hoffmann[1,*], Maxim A. X. Tollenaere[1,*], Teresa Ho[1,2,*], Luis Ignacio Toledo[1], Matthias Mann[3], Simon Bekker-Jensen[1], Markus Räschle[3,4,#], Niels Mailand[1,2,#]

[1]The Novo Nordisk Foundation Center for Protein Research, and [2]Center for Chromosome Stability, Faculty of Health and Medical Sciences, University of Copenhagen, Blegdamsvej 3B, 2200 Copenhagen, Denmark; [3]Department of Proteomics and Signal Transduction, Max Planck Institute of Biochemistry, Am Klopferspitz 18, 82152 Martinsried, Germany; [4]Present address: Department of Molecular Genetics, TU Kaiserslautern, Paul-Ehrlich Strasse 24, 67663 Kaiserslautern, Germany

*Equal contribution. [#]Correspondence and requests for materials to M.R. (email: raeschle@biologie.uni-kl.de) and N.M. (e-mail: niels.mailand@cpr.ku.dk)

Abstract

Activation of the ATR kinase following perturbations to DNA replication relies on a complex mechanism involving ATR recruitment to RPA-coated single-stranded DNA via its binding partner ATRIP and stimulation of ATR kinase activity by TopBP1. Here, we discovered an independent ATR activation pathway in vertebrates, mediated by the uncharacterized protein ETAA1 (Ewing's tumor-associated antigen 1). Human ETAA1 accumulates at DNA damage sites via dual RPA-binding motifs and promotes replication fork progression and integrity, ATR signaling and cell survival after genotoxic insults. Mechanistically, this requires a conserved domain in ETAA1 that potently and directly stimulates ATR kinase activity independently of TopBP1. Simultaneous loss of ETAA1 and TopBP1 gives rise to synthetic lethality characterized by massive genome instability and abrogation of ATR-dependent signaling. Our findings demonstrate that parallel TopBP1- and ETAA1-mediated pathways underlie ATR activation and that their combined action is essential for coping with replication stress.

Introduction

Alterations to the content and organization of cellular genomes, inflicted by numerous genotoxic insults, may lead to pathological conditions such as cancer, premature aging and neurodegeneration[1,2]. To mitigate this threat, cells mount a coordinated DNA damage response (DDR) that promotes repair of DNA lesions and delays cell cycle progression until genome integrity has been restored[3,4]. The phosphatidyl inositol 3' kinase-related kinases ATM and ATR are master organizers of the DDR that trigger damage-specific signaling cascades through direct phosphorylation of large numbers of effector proteins, including the downstream checkpoint kinases Chk1 and Chk2[4-10]. The critical physiological importance of these kinases in protecting genome stability is illustrated by patients with Ataxia telangiectasia and Seckel syndromes, caused by mutations in *ATM* and *ATR*, respectively, which manifest with a range of severe disabilities[11, 12]. Whereas ATM is mainly activated by DNA double-strand breaks (DSBs), ATR is the major kinase responding to replication stress, a potentially deleterious condition defined by a slowdown or block to replication fork progression, which arises frequently from a broad range of perturbations including DNA damage, nucleotide shortage, and replication-transcription collisions[13, 14]. ATR is essential for ensuring the fidelity of DNA replication after such insults, suppressing new origin firing, preventing fork collapse and promoting the restart of stalled forks. Consequently, disruption of the *ATR* gene causes early embryonic lethality in mice[15, 16].

Replication Protein A (RPA)-coated single-stranded DNA (ssDNA) regions generated by uncoupling of replicative helicase and polymerase movements upon fork stalling or by DSB end resection provide a main stimulus for activation of ATR, which is

recruited to these structures via its obligate binding partner ATRIP[17-19]. In parallel, the PCNA-like Rad9-Rad1-Hus1 (9-1-1) complex is loaded onto junctions of ssDNA and double-stranded DNA (dsDNA), leading to recruitment of the multi-BRCT domain-containing protein TopBP1 via Rad9 phosphorylation, the Mre11-Rad50-Nbs1 (MRN) complex, and the RHINO protein[20-25]. TopBP1 directly stimulates ATR kinase activity by means of an ATR-activating domain (AAD) that may promote conformational changes of the ATR kinase domain[26, 27], and whose integrity is essential for viability in mice[28].

While TopBP1 is the only protein known to harbor an AAD in higher eukaryotes, two additional proteins, the Rad9 orthologue Ddc1 and the exonuclease Dna2, also contain AADs in the yeast *S. cerevisiae*[29, 30]. These factors play partially redundant roles in promoting activation of Mec1, the ATR orthologue in budding yeast, and simultaneous knockout of all three AAD-containing proteins is required to abrogate Mec1-dependent checkpoint signaling in S phase[30]. Whether ATR activation in higher eukaryotes involves AAD-containing proteins other than TopBP1 is therefore an important outstanding question. In this study, we demonstrate that the uncharacterized protein ETAA1 (Ewing's tumor-associated antigen 1) is an RPA-binding protein that harbors a potent AAD and operates in parallel with, but independent of, the canonical 9-1-1/TopBP1 axis to promote ATR signaling upon replication stress. Loss of ETAA1 disrupts the integrity of the DNA replication programme, sensitizes cells to replication stress and displays synthetic lethality with TopBP1 depletion, characterized by abrogation of ATR-dependent checkpoint signaling and massive genomic instability. Thus, ATR activation in human cells relies on dual TopBP1- and

ETAA1-mediated pathways whose combined action is essential for coping with replication stress.

Results

Systematic profiling of DNA double-strand break (DSB)-containing chromatin

We recently developed a mass spectrometry-based approach (CHROMASS) to systematically profile protein recruitment to chromatin containing DNA interstrand crosslinks in *Xenopus* egg extracts[31]. To extend these surveys, we applied CHROMASS and label-free mass spectrometry to study protein enrichment dynamics at chromatin modified with nuclease-generated DNA double-strand breaks (DSBs) (Figure 1a). At early time points, we observed strong and near-exclusive enrichment of virtually all known core factors in classical non-homologous end-joining (c-NHEJ), a major DSB repair pathway (Figure 1b,c;Table S1,S2). At later time points, the ssDNA-binding RPA complex (rfa1-3) and known RPA interactors (including ATR-ATRIP, SMARCAL1 (smal1), rfwd3 and helb) also became enriched on the damaged chromatin (Figure 1b,d;Table S1,S2), indicative of progressive DSB end resection. In addition to many established DSB repair factors, these screens revealed potential new components of DNA damage signaling and repair pathways, one of which we characterize below. These data demonstrate that CHROMASS is a powerful method for comprehensive profiling of the dynamic protein landscape at DSB-modified chromatin.

ETAA1 is a potential DDR factor linked to RPA

Among factors showing recruitment to DSB-containing chromatin in the *Xenopus* system, we identified an uncharacterized protein, etaa1, which became markedly enriched on damaged chromatin together with RPA and RPA-binding factors (Figure 1b-d). High sequence coverage allowed robust quantification of etaa1 across the dataset, revealing strikingly similar intensity profiles of etaa1, RPA subunits and known RPA interactors (Figure S1a-c). Moreover, etaa1 showed strong enrichment on undamaged chromatin upon inhibition of DNA polymerases by Aphidicolin (Figure S1d;Table S3), which causes extensive RPA-ssDNA generation through uncoupling of replicative polymerases and helicases[17]. This suggests that the function of etaa1 is tightly linked to RPA.

To characterize the cellular function of etaa1, we focused on the human orthologue, ETAA1 (Ewing's tumor-associated antigen 1), an uncharacterized 926-amino acid protein[32]. When expressed stably in human cells, GFP-tagged ETAA1 underwent prominent redistribution to laser-induced DSBs demarcated by γH2AX positivity (Figure 1e,f). Consistent with the strong clustering of etaa1 with RPA and RPA-interactors in CHROMASS experiments (Figure S1b), ETAA1 was only recruited to DNA damage sites in cells displaying RPA1 accumulation, and the ETAA1 and RPA1 signals perfectly co-localized in a microfoci-like pattern contained within the more expanded γH2AX regions at laser stripes (Figure 1e,f)[33]. ETAA1 also formed nuclear foci colocalizing with RPA after short-term exposure to Camptothecin (CPT), which induces replication-dependent DSBs, and Hydroxyurea (HU), which causes helicase-polymerase uncoupling but little DSB formation (Figure 1g). We conclude that ETAA1 is recruited to RPA-coated ssDNA regions generated upon genotoxic insults in vertebrate cells.

ETAA1 accumulates at DNA damage sites through direct binding to RPA

The observations above suggested that ETAA1 might be recruited to DNA damage sites through direct binding to RPA. Consistently, inhibition of RPA accumulation at DSB sites by knockdown of CtIP, a key factor in DSB end resection[34], or RPA1, suppressed ETAA1 recruitment to damaged DNA, while depletion of core homologous recombination (HR) factors such as BRCA2 or RAD51 had no effect (Figure 2a;S2a). Moreover, ETAA1 and RPA subunits interacted firmly in reciprocal co-immunoprecipitation assays (Figure 2b,c). Expression of a series of ETAA1 fragments showed that its C-terminal portion contained the RPA-binding determinant (Figure S2b). Inspection of the primary sequence of this region revealed an evolutionarily conserved motif in the extreme C-terminus of ETAA1 showing striking homology with the RPA2-binding motifs in SMARCAL1, XPA and TIPIN (Figure 2d)[35-37]. Indeed, removal of the C-terminal region in RPA2 recognized by these motifs impaired its interaction with ETAA1 (Figure 2c). Deletion of the ETAA1 C-terminus containing the putative RPA2-binding motif (ΔRBM2) or point mutations of key conserved residues predicted to impair its functional integrity[35, 36] suppressed the RPA-binding ability of ETAA1 and its recruitment to DSBs (Figure 2b,e,f;S2c-f). However, the ETAA1 ΔRBM2 mutant displayed weak accumulation at DNA damage sites in a small proportion of cells (Figure 2e,f), suggesting that additional sequence determinants in ETAA1 also contribute to its DNA damage recruitment. To this end, we noticed a sequence in the central portion of ETAA1 with similarity to known RPA1-binding motifs in ATRIP, NBS1 and RAD9 (Figure 2d)[38]. While deletion of this sequence alone (ΔRBM1) had no impact on the ability of ETAA1 to interact with RPA and DNA damage sites, simultaneous ablation of both RPA-binding motifs (ΔRBM1+2) fully suppressed ETAA1 recruitment to damaged DNA but did not

impair RPA accumulation (Figure 2b,e,f;S2e,f). These data suggest that ETAA1 contains two RPA-binding determinants that jointly underlie its stable retention at DNA damage sites.

ETAA1 contains an ATR-activating domain

We next asked how ETAA1 functions in the DDR. Strikingly, overexpression of full-length ETAA1 led to strong, pan-nuclear γH2AX positivity independently of its binding to RPA (Figure 3a,b). Instead, deleting N-terminal portions of ETAA1 suppressed its ability to promote γH2AX formation, and overexpression of these regions alone was sufficient to trigger H2AX phosphorylation, similar to the TopBP1 ATR-activating domain (AAD) (Figure 3a,b;S3a,b)[39]. Using ETAA1 deletion constructs, we mapped the minimal γH2AX-promoting determinant in ETAA1 to amino acids 56-220, a conserved region harboring a predicted coiled coil domain (Figure 3a-c;S3a,b). For reasons described below, we refer to this region as AAD (ATR-activating domain) (Figure 3c;S3a). In-frame deletion of this sequence (ΔAAD) had no impact on ETAA1 recruitment to DNA damage sites but abolished γH2AX formation upon ETAA1 overexpression (Figure 3a,b), further suggesting that this activity is uncoupled from its RPA-binding ability. To characterize the ability of ETAA1-AAD to induce γH2AX formation, we fused this sequence to GFP and an estrogen receptor variant (ERT2), allowing for swift nuclear translocation of otherwise cytoplasmic GFP-ETAA1-AAD-ERT2 upon treatment with 4-hydroxy-tamoxifen (4-OHT) (Figure 3c,d). Exposure of cells stably expressing GFP-ETAA1-AAD-ERT2 to 4-OHT triggered rapid and robust pan-nuclear γH2AX positivity irrespective of cell cycle position (Figure 3d-f;S3c). This effect resembled that of an analogous system for 4-OHT-controlled nuclear expression of TopBP1-AAD[39],

however ETAA1-AAD promoted γH2AX formation at lower expression levels than TopBP1-AAD (Figure S3d). Several lines of evidence suggested that similar to TopBP1-AAD[39], the γH2AX positivity caused by ETAA1-AAD overexpression was not a consequence of DNA breakage: First, the ETAA1-AAD-induced γH2AX signal was pan-nuclear rather than focal (Figure 3a,d,e) and it was not accompanied by RPA foci formation and chromatin loading (Figure S3e). Second, treatment with kinase inhibitors or siRNAs showed that the γH2AX-promoting ability of ETAA1-AAD was independent of the DSB-responsive kinases ATM and DNA-PK, whereas the kinase activity of ATR was essential (Figure 3f; see also Figure S6a-c).

Because ATR is capable of phosphorylating H2AX like ATM and DNA-PK[40], these data suggested that ETAA1-AAD directly stimulates ATR kinase activity similar to TopBP1-AAD. Indeed, both full-length ETAA1 and ETAA1-AAD alone interacted with ATR in co-immunoprecipitation assays (Figure 3g;S3f). When incubated with purified ATR-ATRIP complex, recombinant ETAA1-AAD markedly stimulated ATR kinase activity towards MCM2 *in vitro* (Figure 3h), strongly suggesting that this domain is a *bona fide* AAD. The TopBP1-AAD contains a conserved tryptophan residue (W1145 in human TopBP1) that is essential for its ability to stimulate ATR kinase activity[26]. Strikingly, the sequence spanning this residue displayed similarity to a region within ETAA1-AAD, and targeted point mutations of aromatic amino acids in this sequence (AAD^{mut}) were sufficient to abrogate γH2AX formation triggered by overexpression of full-length ETAA1 or its AAD alone (Figure 3a-c;S3a). Interestingly, ETAA1-AAD contains several potential ATR phosphorylation sites and was phosphorylated by ATR *in vitro* (Figure 3h;S3a). Moreover, endogenous ETAA1 showed a prominent ATR-dependent mobility shift after replication stress (Figure

S3g), suggesting that it undergoes phosphorylation by ATR in response to such insults. Finally, mass spectrometry-based analysis of ATR-dependent phosphorylation changes induced by ETAA1-AAD overexpression showed that many ATR phosphorylation sites, including two in ETAA1-AAD itself, were significantly upregulated under these conditions (Figure 3i;S3h,i;Table S4). We confirmed biochemically for H2AX and Chk1 that nuclear overexpression of ETAA1-AAD enhanced their ATR-dependent phosphorylation (Figure 3j). Altogether, these results demonstrate that ETAA1 harbors an AAD capable of directly and potently stimulating ATR kinase activity.

ETAA1 promotes ATR-mediated signaling and cell survival after replication stress

Prompted by the findings above, we generated human HCT116 cell lines with targeted *ETAA1* knockout (*ETAA1Δ*) to investigate whether ETAA1 promotes ATR signaling upon genotoxic stress. Indeed, while ablation of ETAA1 expression did not markedly affect overall cell cycle distribution (Figure S4a), ATR-dependent phosphorylation of RPA2 at S33 in response to CPT treatment was strongly diminished in HCT116 *ETAA1Δ* cells (Figure 4a-c). Likewise, RPA2 S4/S8 phosphorylation, which occurs downstream of S33 phosphorylation in CPT-treated cells[41], was clearly defective in *ETAA1Δ* cells (Figure 4a,b). Similar effects could be seen in HeLa cells ablated for ETAA1 expression (Figure S4b,c). Importantly, ETAA1 knockout did not impair RPA loading at CPT-induced DSBs (Figure 4b-e), suggesting that ETAA1 loss impairs the response to CPT at the level of checkpoint signaling but not ssDNA generation via DSB end resection. In response to HU-induced helicase-polymerase uncoupling, ATR is essential to prevent RPA exhaustion and fork breakage by suppressing new origin firing, and inhibition of ATR in HU-

treated cells therefore leads to excessive DSB formation and RPA hyperphoshorylation[42]. Consistently, HU-treated *ETAA1Δ* cells showed increased levels of RPA2 phosphorylation similar to the effect of ATR inhibition (Figure S4d)[42]. In contrast, ATR-dependent phosphorylation of Chk1 after treatment with CPT or HU was not markedly altered in ETAA1-deficient cells (Figure 4a;S4c), indicating that loss of ETAA1 differentially affects ATR substrates.

Further supporting a role of ETAA1 in promoting ATR signaling, loss of ETAA1 rendered cells highly sensitive to replication stress induced by HU, CPT or Mitomycin C (MMC), but not to clastogens such as Etoposide that generate DSBs independently of replication (Figure 4f-h;S4e-g). Depletion of ETAA1 by siRNAs phenocopied the effect of *ETAA1* knockout in cell survival assays (Figure S4h-j). Importantly, complementation of *ETAA1Δ* cells with ectopic ETAA1 wild-type (WT), but not the ΔRBM1+2, ΔAAD and AAD^{mut} mutants, fully rescued their hypersensitivity to CPT and partially restored survival after HU or MMC (Figure 4f-h;S4k,l). Because ETAA1 is a potent ATR activator, it is possible that expression of stably reconstituted GFP-ETAA1 at levels above that of endogenous ETAA1 (Figure S4k) may adversely affect cellular responses to certain genotoxic agents. We conclude that ETAA1 has an important role in promoting cell survival following replication stress, in a manner that requires both its ATR-activating and RPA-binding abilities.

ETAA1 is required for DNA replication integrity

We performed DNA fiber assays to understand how the absence of ETAA1 sensitizes cells to replication stress. By labeling cells with consecutive pulses of

chlorodeoxyuridine (CldU) and 5'-iododeoxyuridine (IdU), we found that ETAA1 deficiency in both HCT116 and HeLa cells caused a strong reduction in replication fork speed in otherwise unperturbed cells (Figure 5a;S5a). Moreover, ETAA1-deficient cells showed marked asymmetry of bidirectional replication forks from individual replication origins (Figure 5b;S5b), suggesting that ETAA1 loss gives rise to a higher incidence of fork pausing and stalling. The diminished fork speed in *ETAA1Δ* cells was unexpected, given the similar cell cycle and EdU incorporation profiles of WT and *ETAA1Δ* cells (Figure S4a,b). However, we found that in both HCT116 and HeLa *ETAA1Δ* cells, the slower fork progression in *ETAA1Δ* cells was accompanied by a dramatically increased rate of new origin firing (Figure 5c;S5c). Hence, loss of ETAA1 deregulates DNA replication initiation and elongation, similar to reported effects of ATR inhibition[43]. These defects were fully corrected by stably reconstituted WT ETAA1 (Figure 5a-c). Further supporting a key role of ETAA1 in promoting ATR signaling during replication, we found that the basal γH2AX level in unstressed cells, which was ATR-dependent and restricted to S/G2 phase cells, was also prominently reduced in *ETAA1Δ* cells, whereas depletion of TopBP1 had no effect (Figure 5d;S5d-g).

We next assessed how ETAA1 loss affects DNA replication status after fork-stalling insults. When cells were pulse-labeled with CldU and then with IdU in the presence of CPT, ETAA1 was again important for suppressing fork progression defects and new origin firing, in an AAD-dependent manner (Figure 5e,f). In separate experiments, we found that *ETAA1Δ* cells subjected to prolonged low-dose treatment with the DNA polymerase inhibitor Aphidicolin showed markedly elevated levels of abnormal nuclei and micronuclei as well as 53BP1 nuclear bodies in G1 phase[44]

(Figure 5g,h), further demonstrating a compromised ability of these cells to respond to replication problems. These data show that like ATR, ETAA1 is important for the integrity of DNA replication during both unperturbed and stressful conditions.

ETAA1 and TopBP1 function in independent but parallel ATR activation pathways

Because both ETAA1 and TopBP1 contain AADs, we reasoned that they might cooperatively promote ATR-dependent signaling after replication stress. We therefore asked whether they function in joint or separate ATR activation pathways. Knockdown of TopBP1 or the 9-1-1 subunit Rad9 had no effect on the ability of ETAA1-AAD to stimulate ATR kinase activity (Figure S6a-c). Likewise, ETAA1 did not impair the ability of TopBP1-AAD to enhance ATR activity (Figure S6d), suggesting that ETAA1 and TopBP1 function in independent ATR activation pathways. Remarkably, however, whereas individual depletion of TopBP1 or ETAA1 from HCT116 cells only had a modest impact on cellular fitness, simultaneous loss of these proteins profoundly impaired cell proliferation (Figure 6a) and led to strongly increased rates of spontaneous DNA breakage in otherwise undamaged cells, as evidenced by neutral comet assays and markers of ATM kinase activity, including H2AX, RPA2 S4/S8 and Chk2 T68 phosphorylation (Figure 6b-e). This phenotype mimicked the effect of persistent ATR inhibition and could be seen in both HCT116 and HeLa *ETAA1Δ* cells, as well as after siRNA-mediated co-depletion of ETAA1 and TopBP1 (Figure 6b-e;S6e-g). Quantitative image analysis revealed that depletion of TopBP1 from *ETAA1Δ* cells led to strongly elevated levels of chromatin-bound RPA accompanied by γH2AX formation (Figure 6c), suggesting that simultaneous loss of ETAA1 and TopBP1 leads to massive replication fork collapse[42]. A substantial proportion of these cells displayed fragmented nuclei with sub-G1 DNA content

(Figure 6c,d;S6h), a phenotype also observed after loss of ATR kinase activity[15, 45]. Cells lacking both ETAA1 and TopBP1 progressed abnormally through mitosis and frequently stained positive for γH2AX and the mitotic marker H3 pS10 (Figure S6i;Video S1,S2), suggesting that they have a defective G2/M checkpoint and enter mitosis prematurely in the presence of DNA damage. In contrast, apoptosis inhibitors did not suppress nuclear fragmentation following combined ETAA1 and TopBP1 loss (Figure S6j), suggesting this phenotype mostly results from mitotic catastrophe. Complementation of *ETAA1Δ* cells with ectopic WT ETAA1, but not AAD- and RPA binding-deficient mutants, reversed Chk2 and RPA2 hyper-phosphorylation resulting from TopBP1 knockdown in this background (Figure 6g). These data suggested that ETAA1 and TopBP1 operate in parallel pathways of ATR regulation, and that their simultaneous inactivation is detrimental to genome integrity and cell survival by causing robust impairment of ATR signaling. Consistently, whereas depletion of ETAA1 or TopBP1 alone did not markedly impact ATR-dependent Chk1 phosphorylation in HCT116 and HeLa cells, simultaneous loss of these proteins strongly reduced Chk1 phosphorylation levels (Figure 6b,g;S6e). Stable expression of ETAA1 WT but not AAD- and RPA binding-deficient mutants restored Chk1 phosphorylation in *ETAA1Δ* cells depleted of TopBP1 (Figure 6g). Finally, *ETAA1Δ* cells were more sensitive to low concentrations of ATR inhibitors than WT cells (Figure 6h), suggesting that loss of ETAA1 decreases the overall cellular capacity to activate ATR. Collectively, these findings suggest that ETAA1 functions in parallel with, but independent of, the canonical TopBP1 pathway in stimulating ATR kinase activity, and that both pathways make important contributions to ATR-mediated responses to replication stress.

ETAA1 and TopBP1 jointly promote ATR signaling in cancer cell lines

To further test the emerging model of ATR activation involving parallel TopBP1- and ETAA1-dependent pathways, we analyzed ETAA1 expression status in a panel of human cancer cell lines. While the abundance of ETAA1 showed considerable variation across cell lines, we noted that U2OS osteosarcoma cells express abnormally low levels of ETAA1, which did not reflect reduced abundance of *ETAA1* mRNA compared to other cell lines (Figure 7a;S7a,b). Using the protein synthesis inhibitor Cycloheximide (CHX), we found that unlike in HeLa cells, the halflife of ETAA1 was very short in U2OS cells (Figure S7c), possibly accounting for their low ETAA1 expression levels. This provided a framework to further test the biological relevance of ETAA1 for ATR activation. Strikingly, we found that knockdown of TopBP1 quantitatively suppressed HU-induced Chk1 phosphorylation in U2OS cells but not in HeLa cells that express higher levels of ETAA1 (Figure 7b). In contrast, depleting TopBP1 from U2OS cells stably expressing GFP-ETAA1 had little effect on Chk1 phosphorylation after HU treatment (Figure 7b). Similarly, loss of TopBP1 in U2OS but not HeLa cells markedly impaired ATR-dependent H2AX phosphorylation after HU-induced fork stalling, almost mimicking complete ATR inhibition, and this defect could be at least partially reversed by stable expression of GFP-ETAA1 in U2OS cells (Figure 7b-d). Consistently, combined knockdown of TopBP1 and ETAA1 was necessary to suppress ATR-dependent H2AX phosphorylation after HU treatment in HeLa cells, while depletion of either factor alone had little effect (Figure S7d-f). These findings provide further evidence that ETAA1 and TopBP1 function in independent but converging branches of ATR activation after replication stress (Figure 7e).

Discussion

Detailed insights into the molecular framework governing ATR signaling are central to understanding how cells counteract genetic alterations and severe pathologies that may arise as a consequence. Stimulation of ATR kinase activity depends on AAD-containing proteins, three of which contribute to promoting Mec1/ATR-dependent signaling during S phase in budding yeast[30]. Activation of vertebrate ATR is thought to rely largely on a pathway mediated by TopBP1, the only factor in higher eukaryotes known to harbor an AAD. Here, we have shown that ATR activation is not exclusively mediated by this pathway, but that human cells possess a second ATR-stimulatory mechanism that centers on ETAA1 (Figure 7e), a previously uncharacterized protein that undergoes enrichment at DNA damage sites via dual RPA1- and RPA2-binding motifs and contains a *bona fide* AAD. Similar findings were reported by Cortez and colleagues (Nature Cell Biology, this issue). The ETAA1 AAD is a potent inducer of ATR kinase activation and is essential for the ability of ETAA1 to promote ATR signaling, replication integrity, and cell survival. While the known AADs share little sequence homology, Mec1/ATR activation by these domains involves pairs of aromatic amino acids whose spacing varies substantially among individual AADs[30, 46]. Interestingly, the sequence spanning a conserved aromatic residue within the TopBP1 AAD that is essential for its ability to promote ATR activation[26] shows homology to a region within ETAA1-AAD, point mutations of which prevent ATR activation by full-length ETAA1. Thus, the TopBP1 and ETAA1 AADs likely stimulate ATR kinase activity by analogous mechanisms.

The combination of RPA-binding and AAD motifs within ETAA1 may render it a potent ATR activator by obviating the need for ancillary factors targeting it to ATR-

ATRIP complexes at genotoxic stress sites. Indeed, ETAA1 promotes ATR activation independently of the canonical TopBP1/9-1-1 axis, however it remains to be seen whether ETAA1 collaborates with other factors in this process. Studies in mice have shown that the integrity of the TopBP1 AAD is essential for viability[28]. Our data suggest that the ETAA1 and TopBP1 pathways jointly promote ATR signaling, and that both pathways must be inactivated to robustly suppress ATR kinase activity in cells, illustrated by the synthetic lethality caused by combined ETAA1 and TopBP1 loss. An important question arising from these findings concerns the distribution of labor between TopBP1 and ETAA1 in activating ATR after different genotoxic stimuli. Conceivably, they could act on distinct pools of RPA-ssDNA-bound ATR-ATRIP complexes at DNA damage sites. ETAA1 might be particularly important for stimulating ATR kinase activity when long stretches of RPA-coated ssDNA are produced, such as during DSB end resection, where most ATR-ATRIP would be out of reach of 9-1-1-bound TopBP1 at ssDNA-dsDNA junctions. A similar role in promoting ATR kinase activity away from ssDNA-dsDNA junctions was recently suggested for the MRN component Nbs1, albeit in a manner that required TopBP1[41]. Recent work has shown that two distinct modes of Mec1/ATR signaling exist in yeast, one of which is highly active during normal replication but uncoupled from the canonical replication stress-induced checkpoint signaling pathway involving Mec1/Rad53[47]. It is tempting to speculate that the existence of two AAD-containing proteins in vertebrates may similarly enable different modes of ATR signaling in accordance with the status and integrity of DNA replication.

In preclinical studies, ATR kinase inhibitors have shown promising potential in cancer therapy, exacerbating oncogene-induced replication stress to sensitize cancer

cells but not normal cells to DNA damage[48]. The functional status of ETAA1 in cancer cells, which typically experience high loads of replication stress[49], may be an important determinant of their relative sensitivity to ATR inhibitors, since loss of ETAA1 leads to markedly reduced survival rates after treatment with these agents, particularly at low doses. This may be of clinical relevance, as the levels of ETAA1 expression vary considerably among different cancer cell lines and has important bearings on how ATR-dependent signaling responses are instigated in different genetic backgrounds. Of note, variations in the *ETAA1* locus are associated with increased pancreatic cancer risk[50, 51]. By promoting ATR-dependent responses to replication stress, ETAA1 may be an important factor in the cellular defence against cancer and other diseases associated with genomic instability.

Acknowledgements

We thank David Cortez and Akiko Kumagai for providing reagents. We thank Korbinian Mayr, Igor Paron and Gaby Sowa for mass spectrometry support and Martin Steger and Bianca Splettstösser (all from Max Planck Institute of Biochemistry) for experimental advice. This work was supported by grants from The Novo Nordisk Foundation (grants no. NNF14CC0001 and NNF12OC0002114), European Research Council (ERC, grant agreement no. 616236 (DDRegulation)), The Danish Cancer Society, The Danish Council for Independent Research, Danish National Research Foundation (grant no. DNRF115) and Center for Integrated Protein Science Munich (CIPSM). The authors declare no competing financial interests.

Author contributions

PH and NM conceived the study. PH, SH, MAXT and TH designed and performed cell-, biochemistry-, and imaging-based experiments and analyzed the data, under the supervision of NM. MR designed and performed mass spectrometry experiments and analyzed the data, under the supervision of MM. LIT provided help and support with quantitative image analysis and time-lapse microscopy. SB-J co-supervised the study. NM wrote the manuscript with inputs from PH and MR. All authors discussed the results and commented on the manuscript.

Competing financial interests

The authors declare no competing financial interests.

References

1. Hoeijmakers, J.H. Genome maintenance mechanisms for preventing cancer. *Nature* **411**, 366-374 (2001).
2. Lindahl, T. & Barnes, D.E. Repair of endogenous DNA damage. *Cold Spring Harb Symp Quant Biol* **65**, 127-133 (2000).
3. Jackson, S.P. & Bartek, J. The DNA-damage response in human biology and disease. *Nature* **461**, 1071-1078 (2009).
4. Ciccia, A. & Elledge, S.J. The DNA damage response: making it safe to play with knives. *Mol Cell* **40**, 179-204 (2010).
5. Matsuoka, S. *et al.* ATM and ATR substrate analysis reveals extensive protein networks responsive to DNA damage. *Science* **316**, 1160-1166 (2007).
6. Bensimon, A. *et al.* ATM-dependent and -independent dynamics of the nuclear phosphoproteome after DNA damage. *Sci Signal* **3**, rs3 (2010).
7. Beli, P. *et al.* Proteomic investigations reveal a role for RNA processing factor THRAP3 in the DNA damage response. *Mol Cell* **46**, 212-225 (2012).
8. Marechal, A. & Zou, L. DNA damage sensing by the ATM and ATR kinases. *Cold Spring Harbor perspectives in biology* **5** (2013).
9. Liu, Q. *et al.* Chk1 is an essential kinase that is regulated by Atr and required for the G(2)/M DNA damage checkpoint. *Genes Dev* **14**, 1448-1459 (2000).
10. Matsuoka, S., Huang, M. & Elledge, S.J. Linkage of ATM to cell cycle regulation by the Chk2 protein kinase. *Science* **282**, 1893-1897 (1998).
11. O'Driscoll, M., Ruiz-Perez, V.L., Woods, C.G., Jeggo, P.A. & Goodship, J.A. A splicing mutation affecting expression of ataxia-telangiectasia and Rad3-related protein (ATR) results in Seckel syndrome. *Nat Genet* **33**, 497-501 (2003).
12. Shiloh, Y. & Ziv, Y. The ATM protein kinase: regulating the cellular response to genotoxic stress, and more. *Nat Rev Mol Cell Biol* **14**, 197-210 (2013).
13. Zeman, M.K. & Cimprich, K.A. Causes and consequences of replication stress. *Nat Cell Biol* **16**, 2-9 (2014).
14. Cimprich, K.A. & Cortez, D. ATR: an essential regulator of genome integrity. *Nat Rev Mol Cell Biol* **9**, 616-627 (2008).
15. Brown, E.J. & Baltimore, D. ATR disruption leads to chromosomal fragmentation and early embryonic lethality. *Genes Dev* **14**, 397-402 (2000).
16. de Klein, A. *et al.* Targeted disruption of the cell-cycle checkpoint gene ATR leads to early embryonic lethality in mice. *Curr Biol* **10**, 479-482 (2000).
17. Byun, T.S., Pacek, M., Yee, M.C., Walter, J.C. & Cimprich, K.A. Functional uncoupling of MCM helicase and DNA polymerase activities activates the ATR-dependent checkpoint. *Genes Dev* **19**, 1040-1052 (2005).
18. Zou, L. & Elledge, S.J. Sensing DNA damage through ATRIP recognition of RPA-ssDNA complexes. *Science* **300**, 1542-1548 (2003).
19. Cortez, D., Guntuku, S., Qin, J. & Elledge, S.J. ATR and ATRIP: partners in checkpoint signaling. *Science* **294**, 1713-1716 (2001).

20. Delacroix, S., Wagner, J.M., Kobayashi, M., Yamamoto, K. & Karnitz, L.M. The Rad9-Hus1-Rad1 (9-1-1) clamp activates checkpoint signaling via TopBP1. *Genes Dev* **21**, 1472-1477 (2007).
21. Lee, J., Kumagai, A. & Dunphy, W.G. The Rad9-Hus1-Rad1 checkpoint clamp regulates interaction of TopBP1 with ATR. *J Biol Chem* **282**, 28036-28044 (2007).
22. Cotta-Ramusino, C. *et al.* A DNA damage response screen identifies RHINO, a 9-1-1 and TopBP1 interacting protein required for ATR signaling. *Science* **332**, 1313-1317 (2011).
23. Duursma, A.M., Driscoll, R., Elias, J.E. & Cimprich, K.A. A role for the MRN complex in ATR activation via TOPBP1 recruitment. *Mol Cell* **50**, 116-122 (2013).
24. Zou, L., Cortez, D. & Elledge, S.J. Regulation of ATR substrate selection by Rad17-dependent loading of Rad9 complexes onto chromatin. *Genes Dev* **16**, 198-208 (2002).
25. Parrilla-Castellar, E.R., Arlander, S.J. & Karnitz, L. Dial 9-1-1 for DNA damage: the Rad9-Hus1-Rad1 (9-1-1) clamp complex. *DNA Repair (Amst)* **3**, 1009-1014 (2004).
26. Kumagai, A., Lee, J., Yoo, H.Y. & Dunphy, W.G. TopBP1 activates the ATR-ATRIP complex. *Cell* **124**, 943-955 (2006).
27. Mordes, D.A., Glick, G.G., Zhao, R. & Cortez, D. TopBP1 activates ATR through ATRIP and a PIKK regulatory domain. *Genes Dev* **22**, 1478-1489 (2008).
28. Zhou, Z.W. *et al.* An essential function for the ATR-activation-domain (AAD) of TopBP1 in mouse development and cellular senescence. *PLoS Genet* **9**, e1003702 (2013).
29. Navadgi-Patil, V.M. & Burgers, P.M. The unstructured C-terminal tail of the 9-1-1 clamp subunit Ddc1 activates Mec1/ATR via two distinct mechanisms. *Mol Cell* **36**, 743-753 (2009).
30. Kumar, S. & Burgers, P.M. Lagging strand maturation factor Dna2 is a component of the replication checkpoint initiation machinery. *Genes Dev* **27**, 313-321 (2013).
31. Raschle, M. *et al.* Proteomics reveals dynamic assembly of repair complexes during bypass of DNA cross-links. *Science* **348** (2015).
32. Borowski, A. *et al.* Structure and function of ETAA16: a novel cell surface antigen in Ewing's tumours. *Cancer Immunol Immunother* **55**, 363-374 (2006).
33. Bekker-Jensen, S. *et al.* Spatial organization of the mammalian genome surveillance machinery in response to DNA strand breaks. *J Cell Biol* **173**, 195-206 (2006).
34. Symington, L.S. & Gautier, J. Double-strand break end resection and repair pathway choice. *Annu Rev Genet* **45**, 247-271 (2011).
35. Mer, G. *et al.* Structural basis for the recognition of DNA repair proteins UNG2, XPA, and RAD52 by replication factor RPA. *Cell* **103**, 449-456 (2000).
36. Ciccia, A. *et al.* The SIOD disorder protein SMARCAL1 is an RPA-interacting protein involved in replication fork restart. *Genes Dev* **23**, 2415-2425 (2009).

37. Unsal-Kacmaz, K. *et al.* The human Tim/Tipin complex coordinates an Intra-S checkpoint response to UV that slows replication fork displacement. *Mol Cell Biol* **27**, 3131-3142 (2007).
38. Xu, X. *et al.* The basic cleft of RPA70N binds multiple checkpoint proteins, including RAD9, to regulate ATR signaling. *Mol Cell Biol* **28**, 7345-7353 (2008).
39. Toledo, L.I., Murga, M., Gutierrez-Martinez, P., Soria, R. & Fernandez-Capetillo, O. ATR signaling can drive cells into senescence in the absence of DNA breaks. *Genes Dev* **22**, 297-302 (2008).
40. Ward, I.M. & Chen, J. Histone H2AX is phosphorylated in an ATR-dependent manner in response to replicational stress. *J Biol Chem* **276**, 47759-47762 (2001).
41. Shiotani, B. *et al.* Two distinct modes of ATR activation orchestrated by Rad17 and Nbs1. *Cell reports* **3**, 1651-1662 (2013).
42. Toledo, L.I. *et al.* ATR prohibits replication catastrophe by preventing global exhaustion of RPA. *Cell* **155**, 1088-1103 (2013).
43. Couch, F.B. *et al.* ATR phosphorylates SMARCAL1 to prevent replication fork collapse. *Genes Dev* **27**, 1610-1623 (2013).
44. Lukas, C. *et al.* 53BP1 nuclear bodies form around DNA lesions generated by mitotic transmission of chromosomes under replication stress. *Nat Cell Biol* **13**, 243-253 (2011).
45. Toledo, L.I. *et al.* A cell-based screen identifies ATR inhibitors with synthetic lethal properties for cancer-associated mutations. *Nat Struct Mol Biol* **18**, 721-727 (2011).
46. Wanrooij, P.H., Tannous, E., Kumar, S., Navadgi-Patil, V.M. & Burgers, P.M. Probing the Mec1ATR Checkpoint Activation Mechanism with Small Peptides. *J Biol Chem* **291**, 393-401 (2016).
47. Bastos de Oliveira, F.M. *et al.* Phosphoproteomics reveals distinct modes of Mec1/ATR signaling during DNA replication. *Mol Cell* **57**, 1124-1132 (2015).
48. Fokas, E. *et al.* Targeting ATR in DNA damage response and cancer therapeutics. *Cancer Treat Rev* **40**, 109-117 (2014).
49. Lopez-Contreras, A.J. & Fernandez-Capetillo, O. The ATR barrier to replication-born DNA damage. *DNA Repair (Amst)* **9**, 1249-1255 (2010).
50. Childs, E.J. *et al.* Common variation at 2p13.3, 3q29, 7p13 and 17q25.1 associated with susceptibility to pancreatic cancer. *Nat Genet* **47**, 911-916 (2015).
51. Wu, C. *et al.* Genome-wide association study identifies five loci associated with susceptibility to pancreatic cancer in Chinese populations. *Nat Genet* **44**, 62-66 (2012).

Figure legends

Figure 1.

Systematic profiling of DSB-containing chromatin reveals ETAA1 as a potential DDR factor

a. CHROMASS workflow to analyze protein recruitment to DSB-containing chromatin. Sperm chromatin was incubated in *Xenopus* egg extract and DSBs induced by addition of PflMI enzyme. After various times, chromatin was isolated by centrifugation through a sucrose cushion and analyzed by label-free mass spectrometry. **b**. Heatmap showing the mean of the z-scored LFQ protein intensities of selected factors for DSB-containing chromatin normalized to the undamaged control (*n*=3). See Table S2 for recruitment profiles for all quantified proteins. **c**. Protein recruitment to DSB-containing chromatin at 15 min compared to an undamaged control. The volcano plot shows the mean difference of the protein intensity (log2) plotted against the p-value resulting from a one-sided modified t-test (see Methods, *n*=3 for both groups). Dashed line indicates the significance cut-off. **d**. Protein recruitment to DSB-containing chromatin at 45 min, plotted as in (c). **e**. U2OS cells stably expressing GFP-ETAA1 were subjected to laser microirradiation, fixed 1 h later and co-immunostained with RPA1 and γH2AX antibodies. **f**. Quantification of data in (e) (mean±SD;*n*=3; 80 cells analyzed per experiment). **g**. U2OS cells stably expressing GFP-ETAA1 were treated with CPT (1 h) or HU (3 h), fixed and co-immunostained with RPA1 and γH2AX antibodies. All scale bars, 10 μm. Data are representative of three (**e**) and two (**g**) independent experiments with similar results.

Figure 2.

ETAA1 is recruited to DNA damage sites through interaction with RPA

a. Representative images of U2OS cells stably expressing GFP-ETAA1 that were transfected with indicated siRNAs and subjected to laser microirradiation, followed by co-immunostaining with RPA1 and γH2AX antibodies. Knockdown efficiency of siRNAs is shown in Figure S2a. **b**. U2OS cells transfected with constructs encoding indicated versions of GFP-ETAA1 or empty vector (EV) were subjected to GFP immunoprecipitation (IP) followed by immunoblotting for the indicated proteins. **c**. As in (b), except that cells were transfected with indicated GFP-RPA2 constructs or empty vector (EV). SMARCAL1 is a positive control for RPA2 binding. **d**. Schematic diagram of human ETAA1 protein, indicating the locations of conserved RPA1- and RPA2-binding motifs (RBM1 and RBM2). Alignments of these sequences with RPA1/2-binding motifs from other proteins are shown. Conserved key residues within the RPA-binding motifs are highlighted. **e**. Representative images of U2OS cells stably expressing wild-type (WT) and mutant forms of GFP-ETAA1 subjected to laser microirradiation followed by immunostaining with γH2AX antibody. **f**. Quantification of data in (e) (mean±SD;*n*=3; approx. 200 cells counted per condition). All scale bars, 10 μm. Data are representative of three (**a**,**b**,**e**) and two (**c**) independent experiments with similar results. Uncropped blots (**b**,**c**) are shown in Figure S8.

Figure 3.

ETAA1 contains an ATR-activating domain (AAD)

a. U2OS cells transfected with indicated GFP-ETAA1 constructs or empty vector (EV) expressing GFP only were immunostained with γH2AX antibody. **b**. Quantification of data in (a) (mean±SD;*n*=3; 240 cells counted per condition). **c**. Schematic diagram of human ETAA1 protein, indicating location of the ATR-

activating domain (AAD), its sequence similarity to the TopBP1 AAD, and the construct used for inducible nuclear translocation of ETAA1-AAD upon 4-OHT treatment. **d**. U2OS cells expressing GFP-ETAA1-AAD-ERT2 were treated or not with 4-OHT for 2 h and immunostained with γH2AX antibody. **e**. Cells in (d) were analyzed by quantitative imaging (bottom). Representative images are shown (top). **f**. As in (e), except that cells were treated with indicated kinase inhibitors 10 min before addition of 4-OHT for 1 h (mean±SD;*n*=3; >3000 cells analyzed per condition). **g**. U2OS cells transfected with empty vector (EV) or GFP-ETAA1 expression construct were subjected to GFP immunoprecipitation (IP) followed by immunoblotting for the indicated proteins. **h**. *In vitro* kinase assay, using purified ATR-ATRIP complex, recombinant ETAA1-AAD and MCM2(79-138) fragments (the latter serving as ATR model substrate) and radioactive ATP (^{32}P). Reactions were resolved on SDS-PAGE, stained with Colloidal Blue (CB), and ^{32}P incorporation was assessed by autoradiography. **i**. Phospho-proteomic analysis of SILAC-labeled U2OS/GFP-ETAA1-AAD-ERT2 cells treated or not with 4-OHT for 2 h to monitor phosphorylation changes triggered by forced nuclear expression of ETAA1-AAD. To identify ATR-dependent changes, ATR inhibitor (ATRi) or vehicle was added 15 min before 4-OHT treatment in an independent SILAC experiment (see Figure S3h for experimental set-up). Scatterplot shows the log2 of mean SILAC ratios from four independent replicates of each experiment plotted against each other (see Table S4 for full data). **j**. Immunoblot analysis of U2OS/GFP-ETAA1-AAD-ERT2 cells treated with 4-OHT for indicated times in the absence or presence of ATR inhibitor (ATRi). All scale bars, 10 μm. Data are representative of three (**a**,**d**,**e**,**h**) and two (**g**,**j**) independent experiments with similar results. Uncropped blots (**g-j**) are shown in Figure S8.

Figure 4.

ETAA1 promotes cell survival and ATR signaling after replication stress

a. Immunoblot analysis of parental HCT116 (WT) cells and derivative *ETAA1* knockout lines (*ETAA1Δ*) exposed to CPT for various times. Asterisk demarcates an unspecific band detected by the ETAA1 antibody. **b**. Chromatin-enriched and soluble fractions of HCT116 WT and *ETAA1Δ* cell lines left untreated or exposed to CPT for 90 min were immunoblotted with indicated antibodies. **c**. HCT116 WT and *ETAA1Δ* cell lines left untreated or exposed to CPT were co-immunostained with RPA2 and RPA2-pS4/S8 antibodies. **d**. As in (c), except that cells were co-immunostained with γH2AX and RPA1 antibodies. **e**. Quantification of data in (d). γH2AX-negative and -positive cell populations were gated and analyzed for mean RPA1 chromatin loading per nucleus by quantitative imaging. Box plot shows median, upper and lower quartiles, 95% values (whiskers) and outliers (n=2000 cells per condition). **f**. Clonogenic survival of HCT116 WT, HCT116 *ETAA1Δ*, and HCT116 *ETAA1Δ* cells stably reconstituted with GFP-ETAA1 that were subjected to various doses of HU for 24 h (mean±SEM;n=3). **g**. As in (f), except that cells were subjected to indicated doses of MMC (mean±SEM;n=3). **h**. As in (f), except that cells were treated with indicated doses of CPT (mean±SEM;n=3). All scale bars, 10 μm. Data are representative of three (**a**,**b**) and two (**c**-**e**) independent experiments with similar results. Uncropped blots (**a**,**b**) are shown in Figure S8.

Figure 5.

ETAA1 promotes DNA replication integrity during unperturbed and stressful conditions

a. DNA fiber analysis of HCT116 WT and *ETAA1Δ* cells labeled with CldU (20 min; red) followed by IdU (20 min; green). Fork speeds were calculated as length of labeled track divided by pulse time. Red bars denote median fork speed (400 fibers, pooled from two independent experiments, analyzed per condition). Representative fibers are shown. **b**. Fork symmetry was calculated as the percentage of shorter divided by longer tracks from (a). Concordance is 100%, representing fully bidirectional replication and equal rates of elongation for both daughter forks. Red bars denote median fork symmetry rate (50 bidirectional forks, pooled from two independent experiments, analyzed per condition). Representative fibers displaying fork symmetrical and asymmetrical bidirectional replication forks are shown. **c**. As in (a), except that the proportion of new origins (IdU-only tracks) was determined (200 fibers analyzed per condition per experiment). **d**. Quantitative image analysis of HCT116 cells treated with indicated siRNAs and immunostained with γH2AX antibody. The proportion of γH2AX-positive cells (pink, arbitrary cut-off) is indicated (*n*=2000 cells per condition). **e**. DNA fiber analysis of HCT116 WT and *ETAA1Δ* cells labeled with CldU (20 min) followed by IdU and CPT (40 min). New origin firing was determined as in (c) (200 fibers analyzed per condition per experiment). **f**. Fork progression (CldU- and IdU-positive tracks) in cells from (e). **g**. HCT116 WT and *ETAA1Δ* cells left untreated or grown in the presence of Aphidicolin (0.2 μM) for 24 h were stained with DAPI, and nuclear aberrations (right, representative examples) were assessed (mean±SD;*n*=3; at least 200 cells were counted per condition). **h**. As in (g), except that cells were co-immunostained with 53BP1 and Cyclin A antibodies. 53BP1 bodies in Cyclin A-negative (G1 phase) cells (representative examples shown, right) were enumerated (red lines, median; 150 cells analyzed per condition). Data are

representative of three (**d**,**g**,**h**) independent experiments with similar results. Source data (**a-c**,**e**,**f**,**h**) are provided in Table S5.

Figure 6.

ETAA1 and TopBP1 promote parallel, but independent, pathways of ATR activation

a. Colony formation assay, using HCT116 WT and *ETAA1Δ* cell lines transfected with non-targeting control (CTRL) or TopBP1 siRNAs (mean±SD;*n*=3). **b**. Immunoblot analysis of HCT116 WT and *ETAA1Δ* cells transfected with TopBP1 siRNAs for the indicated times. Asterisk demarcates an unspecific band detected by the ETAA1 antibody. **c**. HCT116 WT and *ETAA1Δ* cell lines transfected with non-targeting control (CTRL) or TopBP1 siRNAs were analyzed by quantitive imaging. The color of each dot (cell nucleus) represents the mean γH2AX intensity (low: grey; high: red); >2000 cells analyzed per condition. **d**. Representative images from the experiment shown in (c). Scale bar, 10 μm. **e**. DSB formation in cells in (b) was monitored by the neutral Comet assay. Tail lengths of at least 70 nuclei were measured for each condition. **f**. DNA content of cells in (d) was analyzed by quantitative imaging. The proportion of cells with sub-G1 DNA content (pink) is indicated. **g**. HCT116 WT, HCT116 *ETAA1Δ-1* and HCT116 *ETAA1Δ-1* cells stably reconstituted with indicated GFP-ETAA1 expression constructs were transfected with non-targeting control (−) or TopBP1 siRNA and immunoblotted with indicated antibodies. **h**. Viability of HCT116 WT and *ETAA1Δ* cell lines grown in the presence of various doses of ATR inhibitor (ATRi) was assayed by measuring cell growth with the SRB assay (mean±SD;*n*=3). *p<0.05, multiple t-test corrected with Holm-Sidak

method. Data are representative of three (**b**,**d**,**f**,**g**) and two (**c**,**e**) independent experiments with similar results. Source data (**e**) are provided in Table S5. Uncropped blots (**b**,**g**) are shown in Figure S8.

Figure 7.

ETAA1 and TopBP1 both contribute to ATR signaling in cancer cell lines

a. Immunoblot analysis of ETAA1 and other proteins involved in ATR activation in indicated exponentially growing human cancer cell lines and Tig3 diploid embryonic lung fibroblasts. **b**. HeLa, U2OS and U2OS/GFP-ETAA1 cells were transfected with TopBP1 siRNAs, treated with HU for 3 h and processed for immunoblotting with indicated antibodies. **c**. HeLa and U2OS cells transfected with indicated siRNAs were treated with HU and ATR inhibitor (ATRi) for 3 h as indicated. Cells were then co-immunostained with γH2AX and RPA1 antibodies and analyzed by quantitative imaging (*n*=1500 cells per condition). The contribution of ATR to the γH2AX signal, based on the ATRi-treated sample, is indicated in blue. Cells displaying maximal HU-induced RPA chromatin loading accompanied by ATM-dependent but ATR-independent H2AX hyperphosphorylation reflecting fork breakage[42] are indicated in pink. **d**. As in (c), but using U2OS and U2OS/GFP-ETAA1 cells (*n*=1500 cells per condition). **e**. Model of parallel ETAA1- and TopBP1-mediated stimulation of ATR kinase activity at RPA-coated ssDNA regions (see main text for details). Change of color represents ATR activation. Data are representative of three (**b**) and two (**a**,**c**,**d**) independent experiments with similar results. Uncropped blots (**a**,**b**) are shown in Figure S8.

Haahr et al. Figure 1

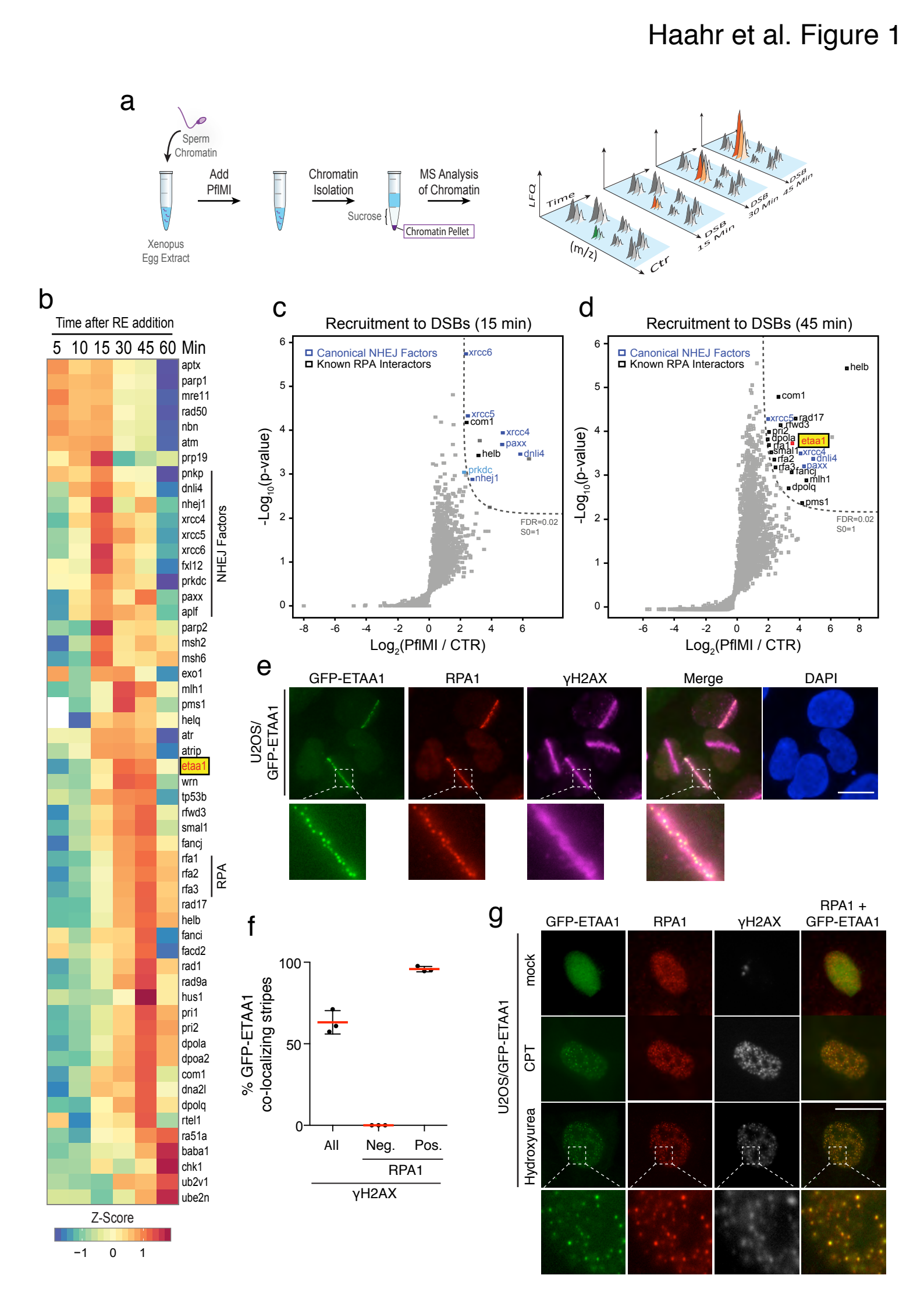

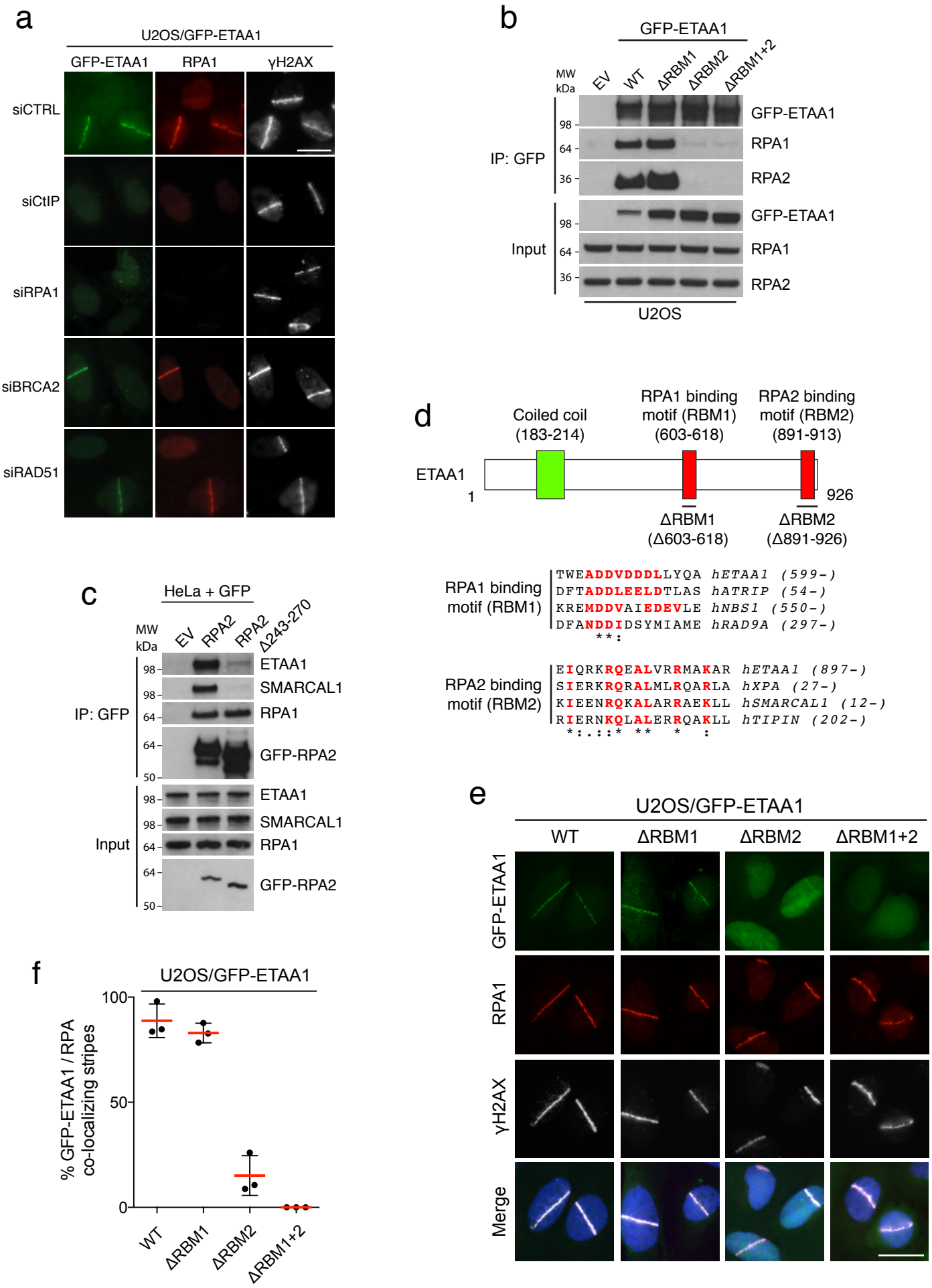
a
U2OS/GFP-ETAA1
GFP-ETAA1
RPA1
γH2AX
siCTRL
siCtIP
siRPA1
siBRCA2
siRAD51
b
GFP-ETAA1
MW kDa
EV
WT
ΔRBM1
ΔRBM2
ΔRBM1+2
IP: GFP
Input
98
64
36
GFP-ETAA1
RPA1
RPA2
U2OS
c
HeLa + GFP
EV
RPA2
RPA2 Δ243-270
ETAA1
SMARCAL1
RPA1
GFP-RPA2
50
d
Coiled coil (183-214)
RPA1 binding motif (RBM1) (603-618)
RPA2 binding motif (RBM2) (891-913)
ETAA1
1
926
ΔRBM1 (Δ603-618)
ΔRBM2 (Δ891-926)
RPA1 binding motif (RBM1)
TWEADDVDDDLLYQA hETAA1 (599-)
DFTADDLEELDTLAS hATRIP (54-)
KREMDDVAIEDEVLE hNBS1 (550-)
DFANDDIDSYMIAME hRAD9A (297-)
RPA2 binding motif (RBM2)
EIQRKRQEALVRRMAKAR hETAA1 (897-)
SIERKRQRALMLRQARLA hXPA (27-)
KIEENRQKALARRAEKLL hSMARCAL1 (12-)
RIERNKQLALERRQAKLL hTIPIN (202-)
e
U2OS/GFP-ETAA1
WT
ΔRBM1
ΔRBM2
ΔRBM1+2
GFP-ETAA1
RPA1
γH2AX
Merge
f
U2OS/GFP-ETAA1
% GFP-ETAA1 / RPA co-localizing stripes
100
50
0
WT
ΔRBM1
ΔRBM2
ΔRBM1+2

Haahr et al. Figure 3

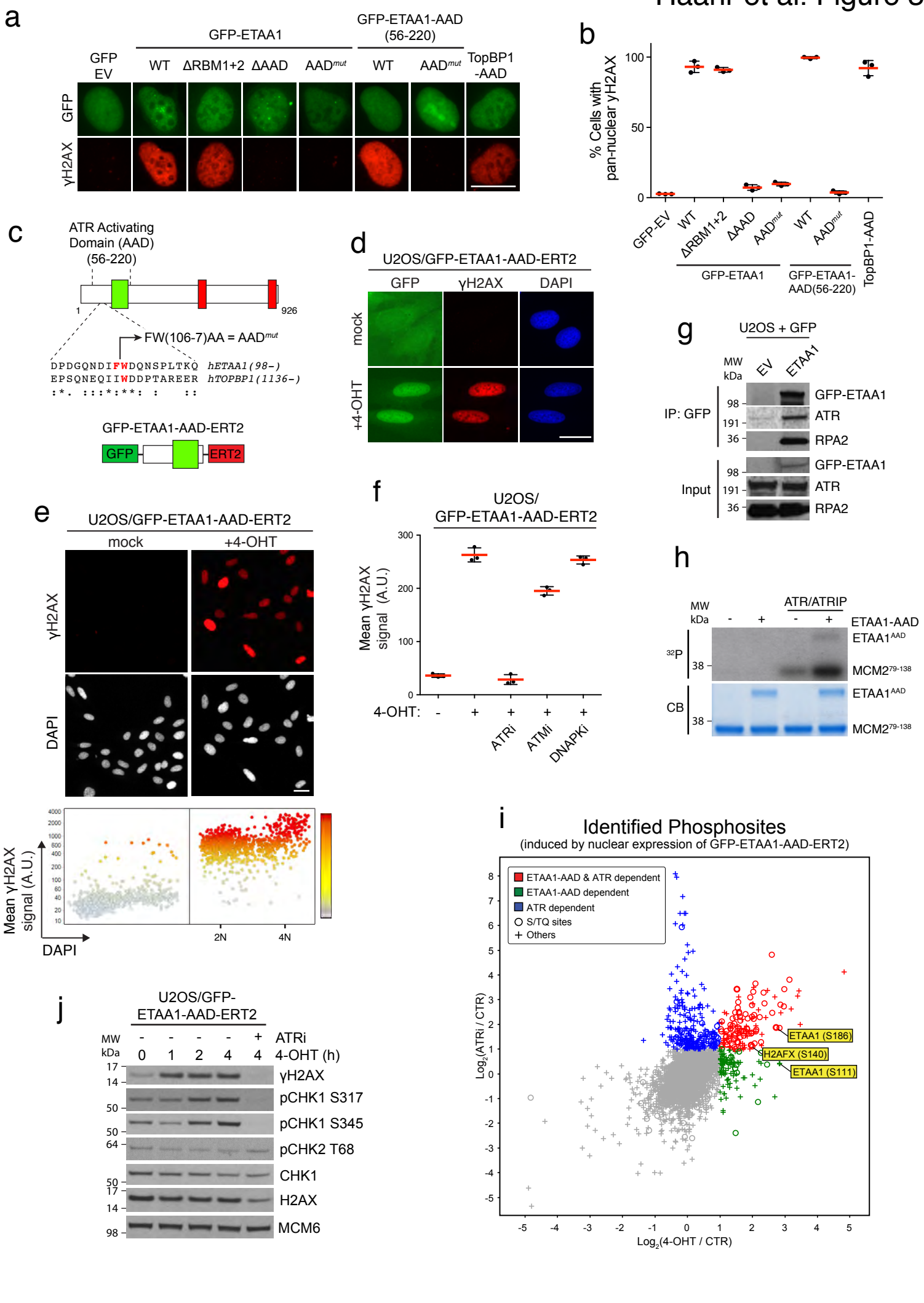

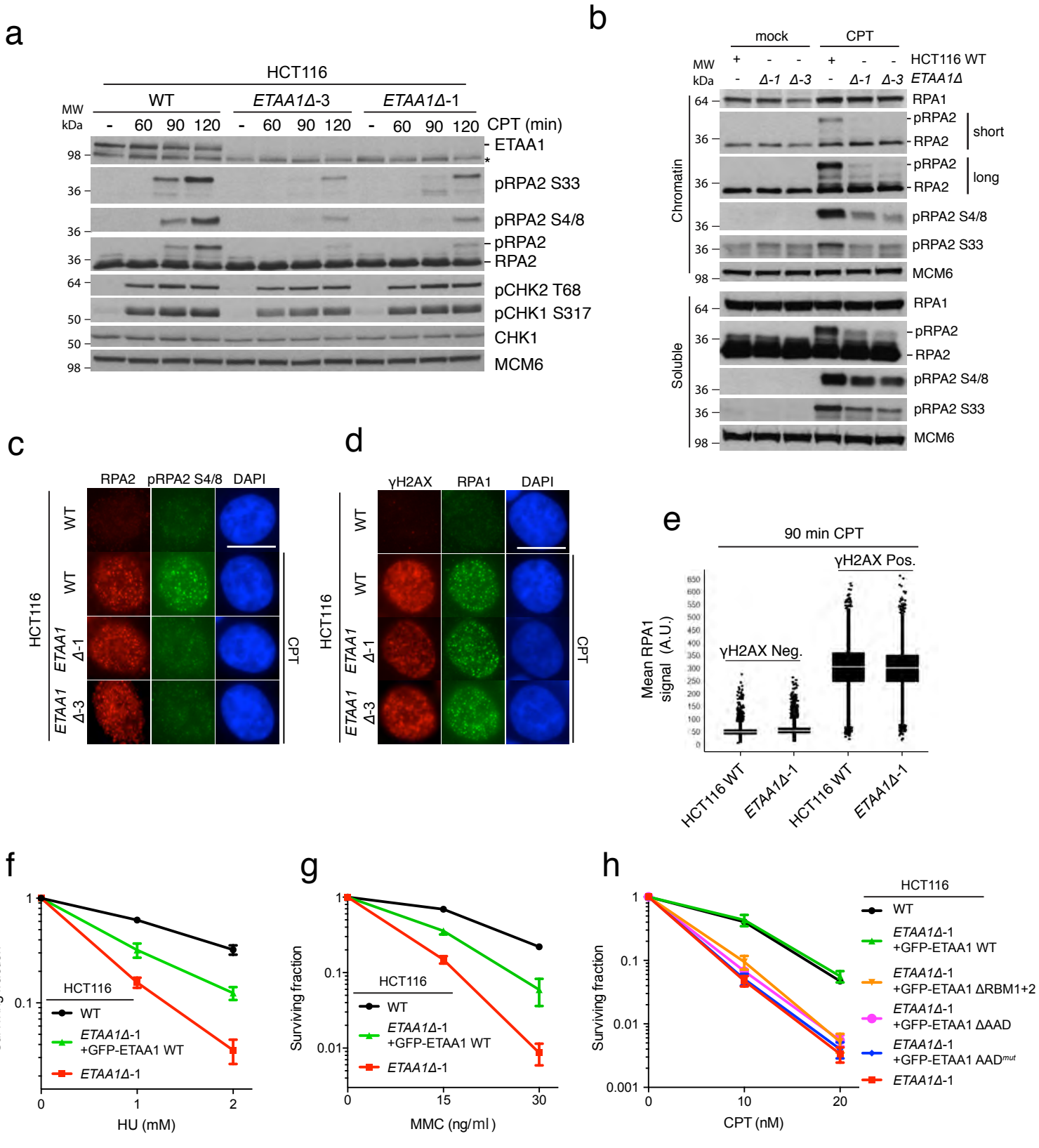
a
HCT116
WT
ETAA1Δ-3
ETAA1Δ-1
MW kDa
- 60 90 120 - 60 90 120 - 60 90 120 CPT (min)
ETAA1
pRPA2 S33
pRPA2 S4/8
pRPA2
RPA2
pCHK2 T68
pCHK1 S317
CHK1
MCM6
b
mock
CPT
HCT116 WT
ETAA1Δ
Chromatin
Soluble
RPA1
pRPA2
RPA2
short
long
pRPA2 S4/8
pRPA2 S33
MCM6
c
RPA2 pRPA2 S4/8 DAPI
HCT116
WT
ETAA1 Δ-1
ETAA1 Δ-3
CPT
d
γH2AX RPA1 DAPI
e
90 min CPT
γH2AX Pos.
γH2AX Neg.
Mean RPA1 signal (A.U.)
HCT116 WT
ETAA1Δ-1
f
Surviving fraction
HU (mM)
WT
ETAA1Δ-1 +GFP-ETAA1 WT
ETAA1Δ-1
g
MMC (ng/ml)
h
CPT (nM)
ETAA1Δ-1 +GFP-ETAA1 ΔRBM1+2
ETAA1Δ-1 +GFP-ETAA1 ΔAAD
ETAA1Δ-1 +GFP-ETAA1 AAD^mut

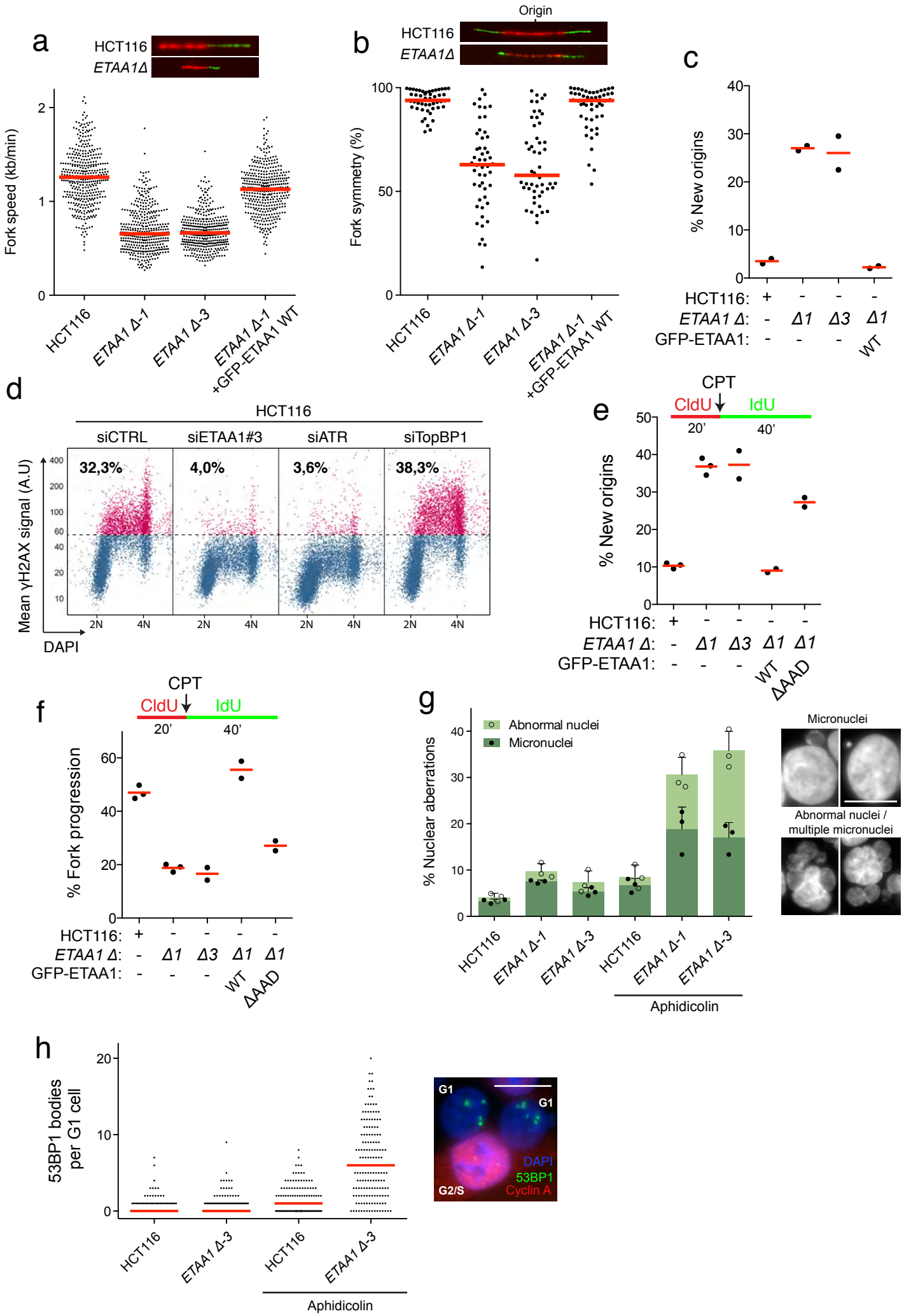
a
HCT116
ETAA1Δ
Fork speed (kb/min)
HCT116
ETAA1 Δ-1
ETAA1 Δ-3
ETAA1 Δ-1 +GFP-ETAA1 WT
b
Origin
HCT116
ETAA1Δ
Fork symmetry (%)
c
% New origins
HCT116: + - - -
ETAA1 Δ: - Δ1 Δ3 Δ1
GFP-ETAA1: - - - WT
d
HCT116
siCTRL
siETAA1#3
siATR
siTopBP1
32,3%
4,0%
3,6%
38,3%
Mean γH2AX signal (A.U)
2N
4N
DAPI
e
CPT
CldU
IdU
20'
40'
% New origins
HCT116: + - - - -
ETAA1 Δ: - Δ1 Δ3 Δ1 Δ1
GFP-ETAA1: - - - WT ΔAAD
f
CPT
CldU
IdU
20'
40'
% Fork progression
HCT116: + - - - -
ETAA1 Δ: - Δ1 Δ3 Δ1 Δ1
GFP-ETAA1: - - - WT ΔAAD
g
Abnormal nuclei
Micronuclei
% Nuclear aberrations
HCT116
ETAA1 Δ-1
ETAA1 Δ-3
Aphidicolin
Micronuclei
Abnormal nuclei / multiple micronuclei
h
53BP1 bodies per G1 cell
HCT116
ETAA1 Δ-3
Aphidicolin
G1
G2/S
DAPI
53BP1
Cyclin A

Haahr et al. Figure 6

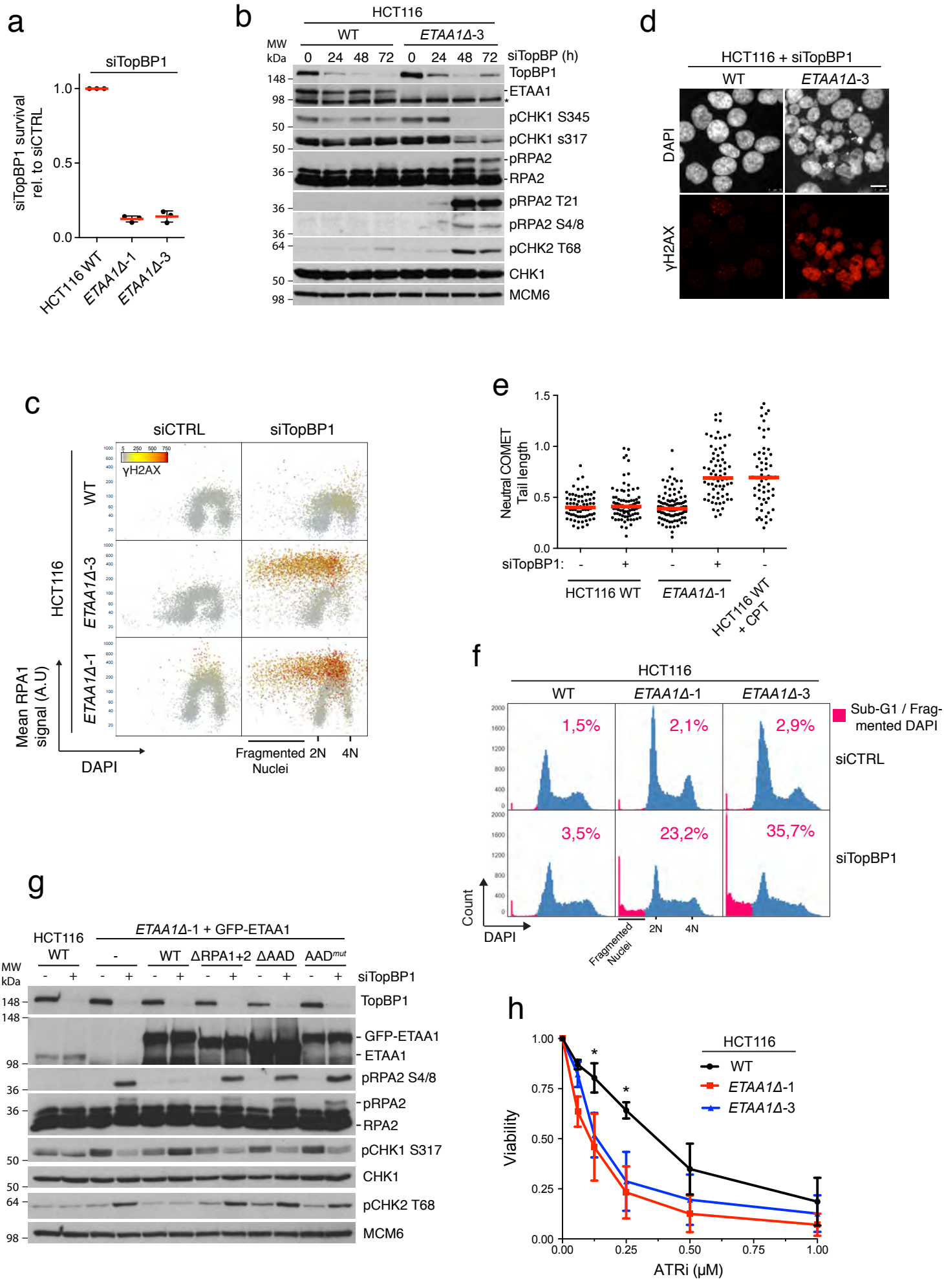

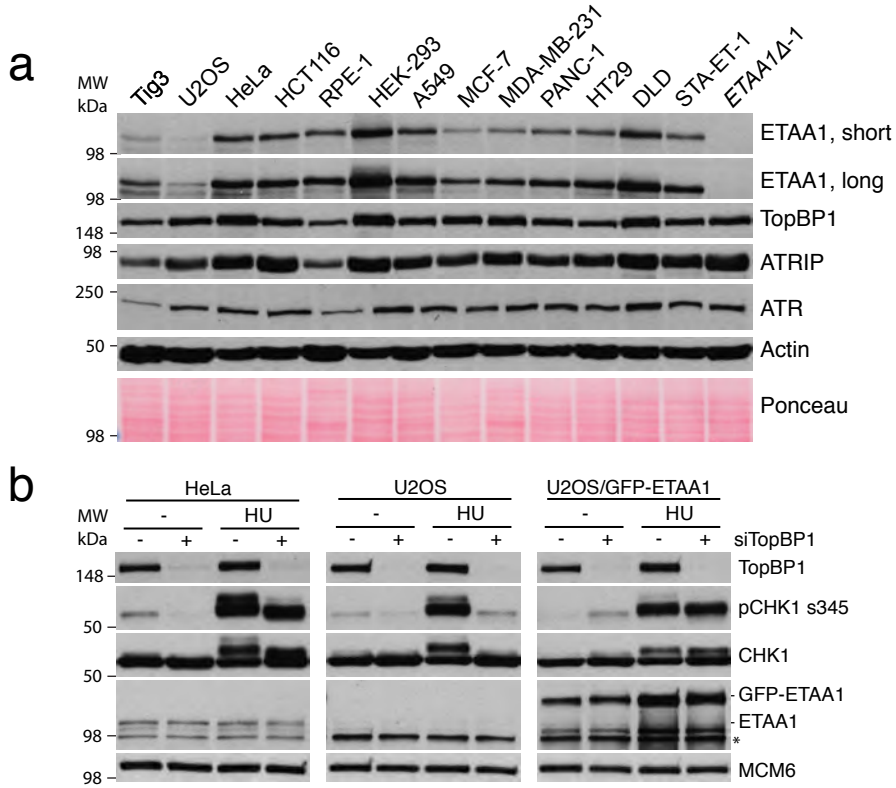
a
MW
kDa
Tig3
U2OS
HeLa
HCT116
RPE-1
HEK-293
A549
MCF-7
MDA-MB-231
PANC-1
HT29
DLD
STA-ET-1
ETAA1Δ-1
98
98
148
98
250
50
98
ETAA1, short
ETAA1, long
TopBP1
ATRIP
ATR
Actin
Ponceau
b
HeLa
U2OS
U2OS/GFP-ETAA1
MW
kDa
-
HU
siTopBP1
148
50
50
98
98
TopBP1
pCHK1 s345
CHK1
GFP-ETAA1
ETAA1
*
MCM6

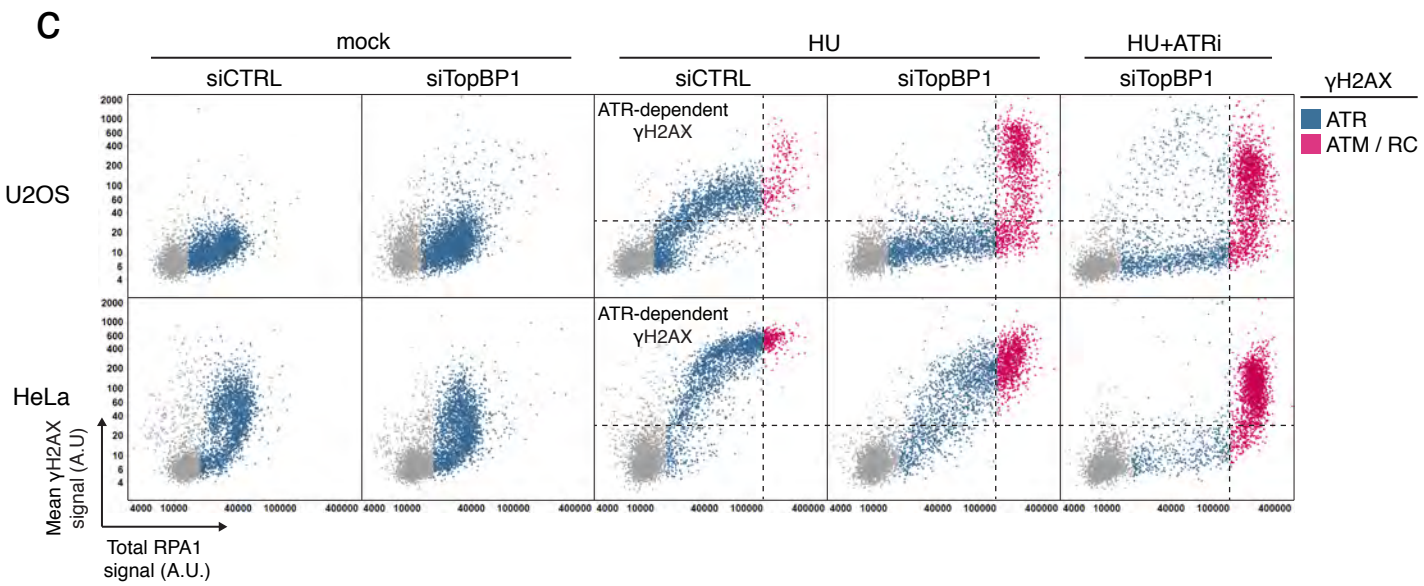
c
mock
HU
HU+ATRi
siCTRL
siTopBP1
siCTRL
siTopBP1
siTopBP1
γH2AX
ATR
ATM / RC
U2OS
HeLa
ATR-dependent
γH2AX
Mean γH2AX
signal (A.U)
Total RPA1
signal (A.U.)

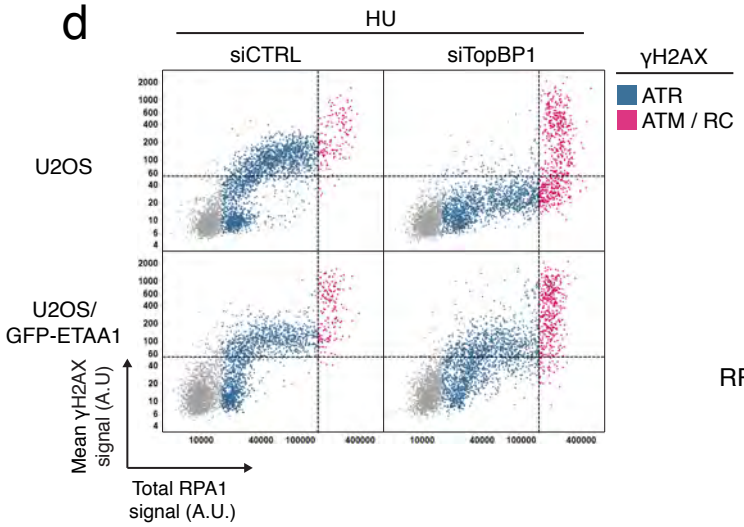
d
HU
siCTRL
siTopBP1
γH2AX
ATR
ATM / RC
U2OS
U2OS/
GFP-ETAA1
Mean γH2AX
signal (A.U)
Total RPA1
signal (A.U.)

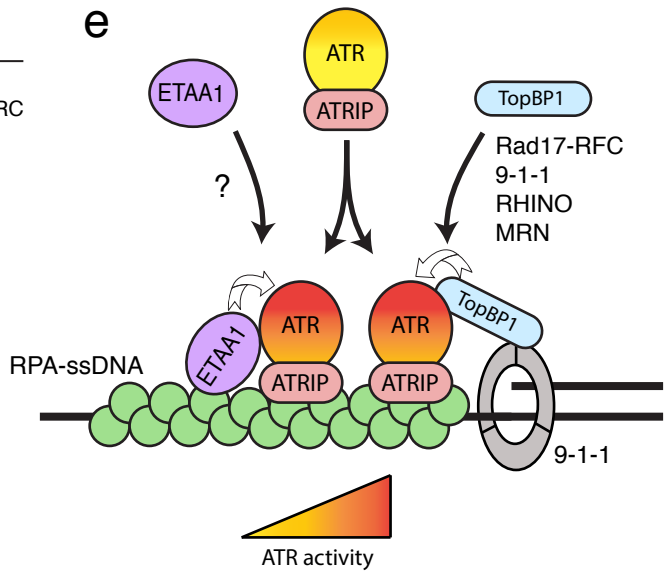
e
ETAA1
ATR
ATRIP
TopBP1
?
Rad17-RFC
9-1-1
RHINO
MRN
RPA-ssDNA
ETAA1
ATR
ATR
TopBP1
ATRIP
ATRIP
9-1-1
ATR activity

Haahr et al. Figure S1

a

>xlEtaa1

MFKQRAGAAGCVKKVGSVPREAGLSGESSSYKKTPKRLSRSKHSSPAFSSPSNDVDQQHEII
WDPYSPTAFKIENGRRKRPNANKCTVEISDIVNRIAPKNEKPADAAYLQMWIGDDAIPSTPVVA
RSRSKASLRPRSLHTEEELMKLARQFDRNLIEAIQPQEQRDLSADEKTVPLGTAQIYETDTFLED
IPEEDVELALKSVSQSSGISTSSHGQKAVDQDAEAALNALFDCSTQKVSGRLSQTLSDISIGSTH
GLHVSVKGNTGEVSLSEKSDGNKFETPTVSKRNTSHSESNSNVLHTSKRDGSILPKEKSRQTE
SHGVSDPAAAISNSQDDFEDDWGNDLFEDDSFVMEITQNPNLIATPKTERTNSKSEQSGLYSV
GSKSFENNKCNDKSVVPNKANHFKFVSRTSNVPVDSHSVGKRDNNISVPSICNVSQLPLNSQN
NNSVQNRRMQSNSSLVPEKDAFTRGLSKNHSTNAEMLGLLNVPAKPSHCHVPQKQNHAPIPE
KASVQLDEWDDPKFSDDVLDMFCKSDSLWETNEDDDDLLYQVCDDVERLTQAQISNEGVNK
MENTQVTSLSGAKTVPGITKQVQPSQHFGQNKNGSQIRQFSSSATNKFSGNATRYNSSTNSSL
QKITAPSAGTGLRVCGNAFTFNENGGLSKTNPAPVKFGRFNSVPSASECTKTLFIGTQSQSMG
NPQAATTSAKSSMAPSKFTFTRTKSSPIVPSHTCTGGTSDFKYMDSQEVAGNKNHKNQLVPKN
ELLNQPFNLKRQLSDSVLQSTKVFVSEERNKKCSMEEIERKKQEALARRQKRLHVLSGETAHP

Sequence Coverage: 52.3%

b

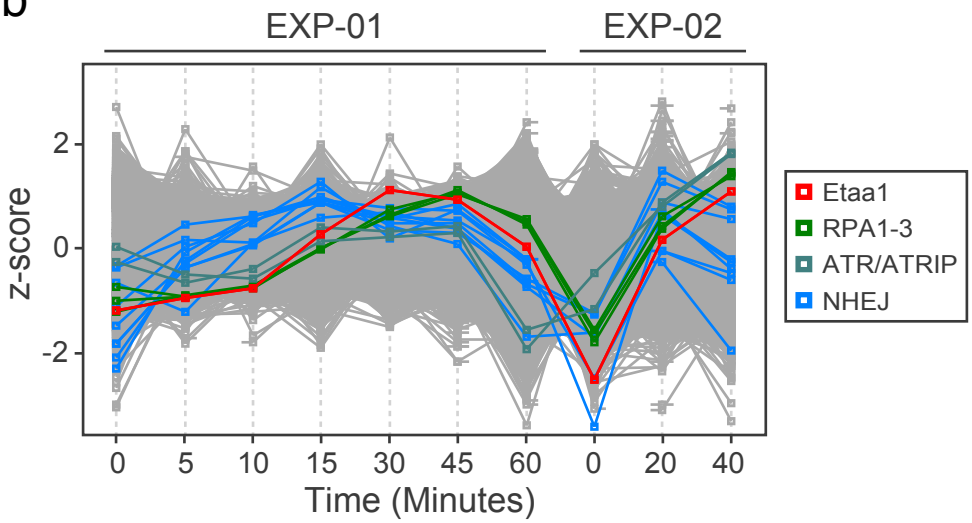

c

Rank	Distance	Protein
1	0.0006	rfa1
2	0.0051	rfa2
3	0.0053	rfa3
4	0.0120	dpoa2
5	0.0363	helb
6	0.0388	nsrp1
7	0.0413	rad9a
8	0.0421	dpolq
9	0.0430	dpola
10	0.0474	etaa1
11	0.0504	pri1
12	0.0610	smal1
13	0.0705	rtel1
14	0.0728	com1
15	0.0787	pri2
16	0.0792	helq
17	0.0802	rad17
18	0.0807	wrn
19	0.0868	mlh1
20	0.0971	fancj
21	0.1026	rad1
26	0.1204	dna2l
33	0.1587	rfwd3

Total: 2668 Profiles

d

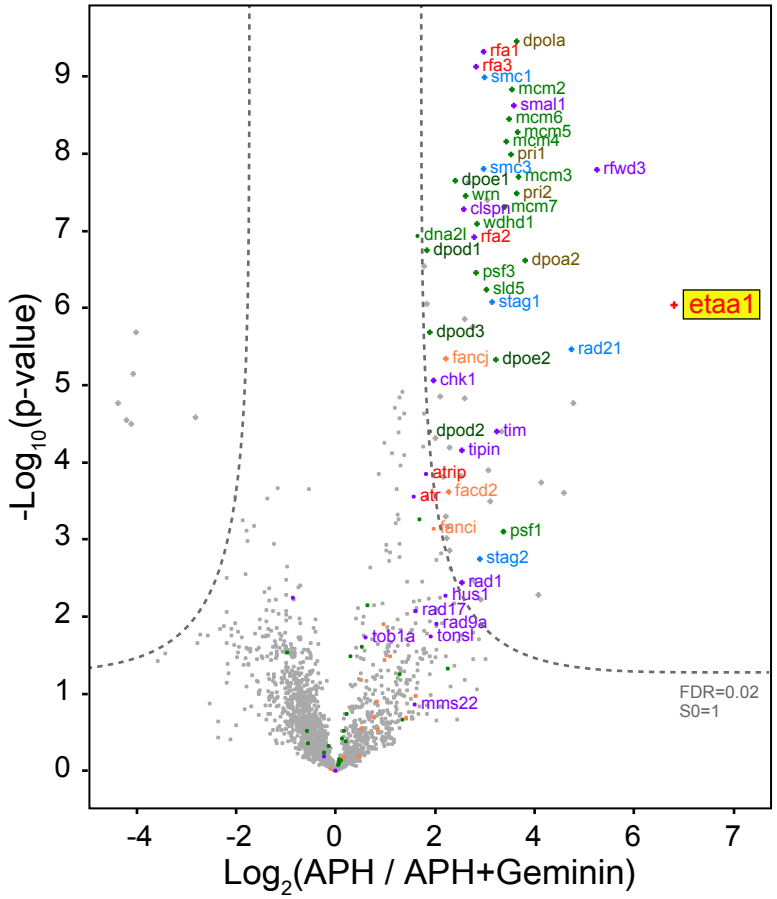

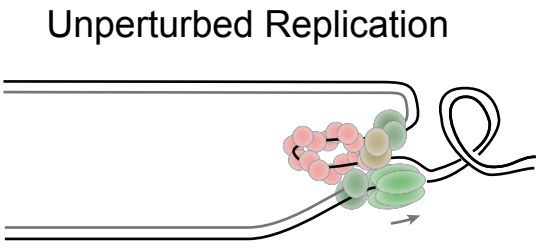

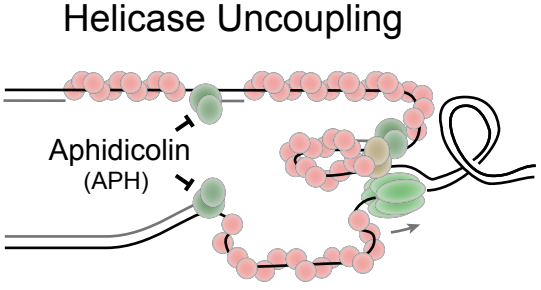

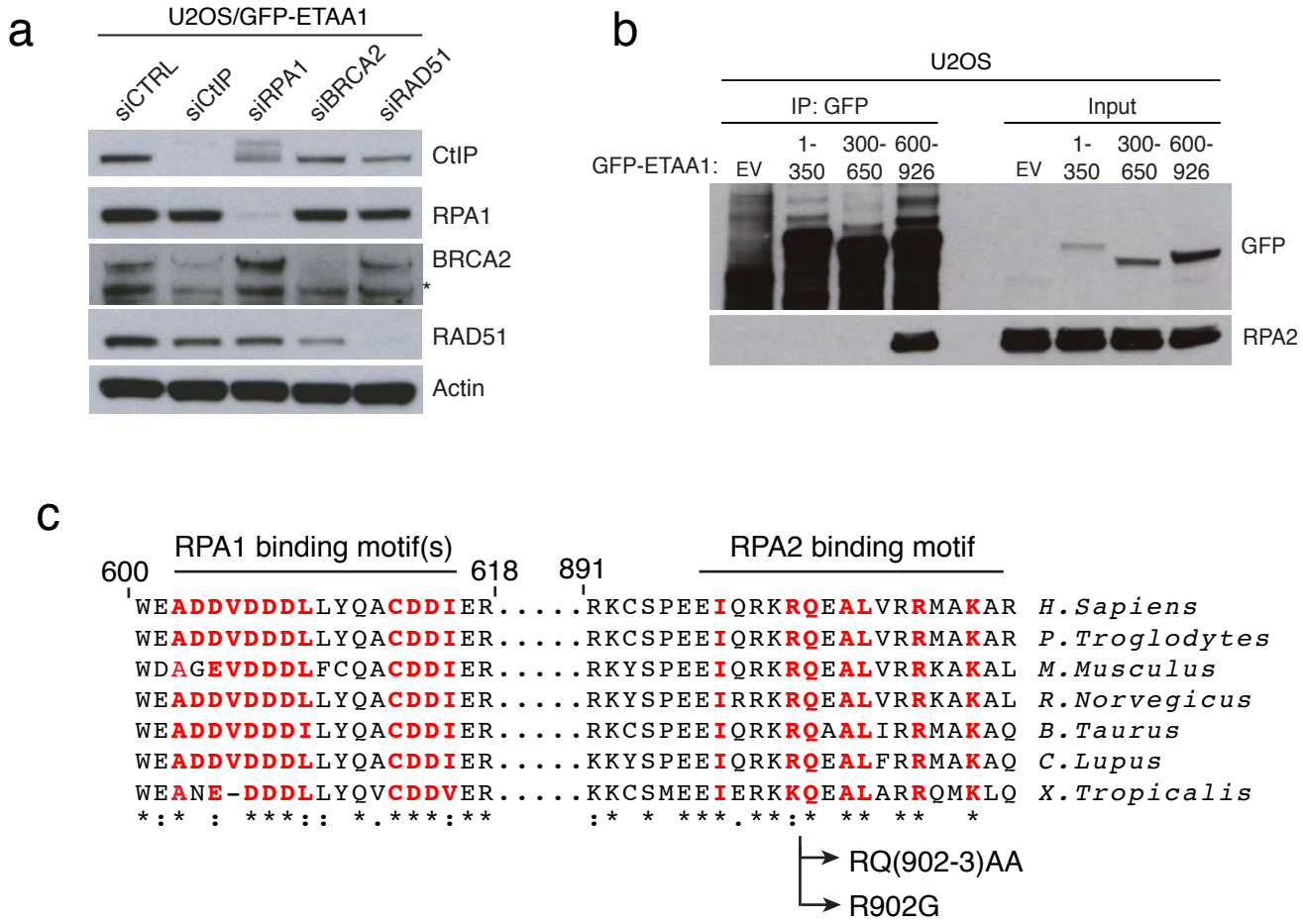
a
U2OS/GFP-ETAA1
siCTRL
siCtIP
siRPA1
siBRCA2
siRAD51
CtIP
RPA1
BRCA2
*
RAD51
Actin
b
U2OS
IP: GFP
Input
GFP-ETAA1:
EV
1-350
300-650
600-926
GFP
RPA2
c
RPA1 binding motif(s)
RPA2 binding motif
600
618
891
WEADDVDDDLLYQACDDIER.....RKCSPEEIQRKRQEALVRRMAKAR H.Sapiens
WEADDVDDDLLYQACDDIER.....RKCSPEEIQRKRQEALVRRMAKAR P.Troglodytes
WDAGEVDDDLFCQACDDIER.....RKYSPEEIQRKRQEALVRRKAKAL M.Musculus
WEADDVDDDLLYQACDDIER.....RKYSPEEIRRKRQEALVRRKAKAL R.Norvegicus
WEADDVDDDILYQACDDIER.....RKCSPEEIQRKRQAALIRRMAKAQ B.Taurus
WEADDVDDDLLYQACDDIER.....KKYSPEEIQRKRQEALFRRMAKAQ C.Lupus
WEANE-DDDLLYQVCDDVER.....KKCSMEEIERKKQEALARRQMKLQ X.Tropicalis
RQ(902-3)AA
R902G
d
U2OS/GFP-ETAA1
WT
RQ(902-3)AA
R902G
GFP-ETAA1
γH2AX
e
WT
ΔRBM1
ΔRBM2
ΔRBM1+2
GFP-ETAA1
Actin
U2OS/GFP-ETAA1
f
U2OS/GFP-ETAA1
WT
ΔRBM1
ΔRBM2
ΔRBM1+2
GFP-ETAA1
RPA1

Haahr et al. Figure S3

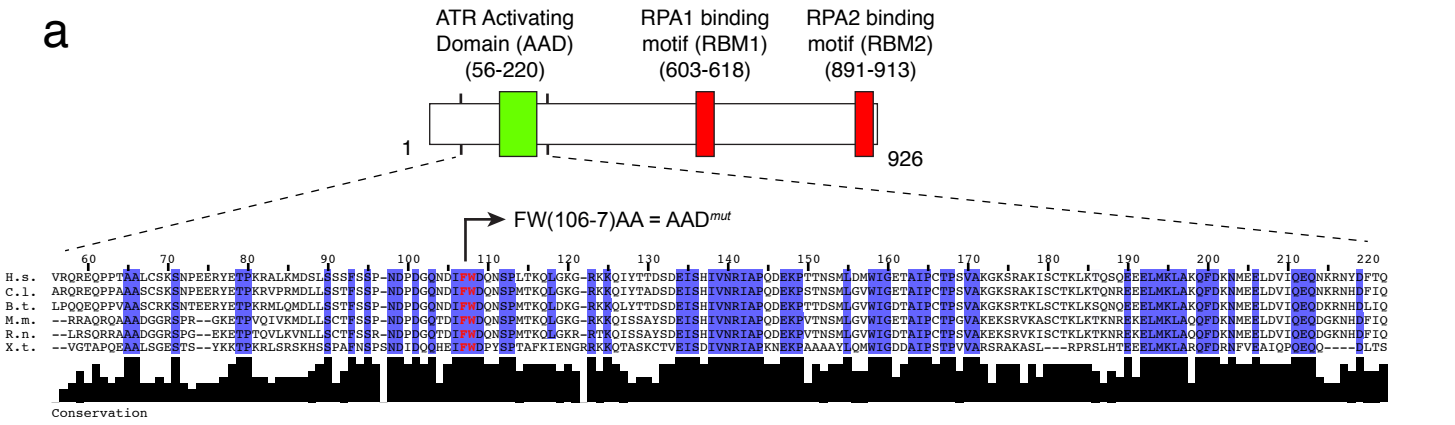

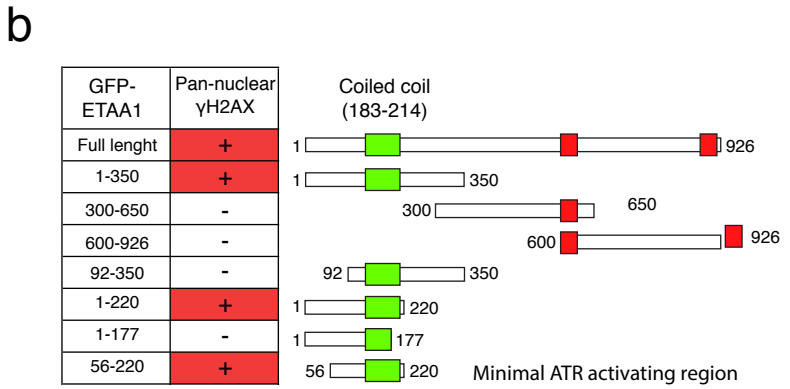

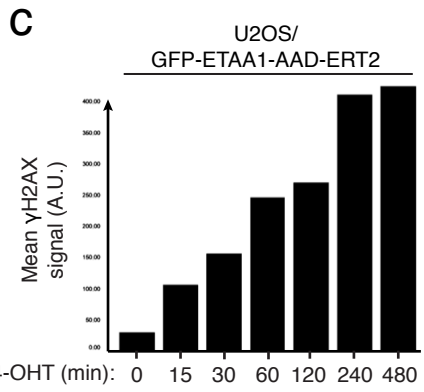

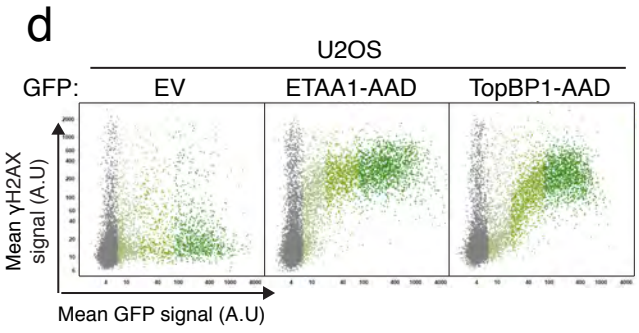

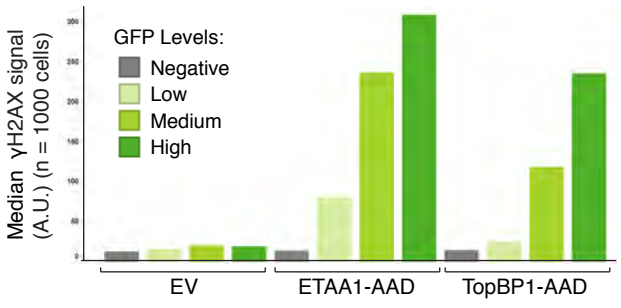

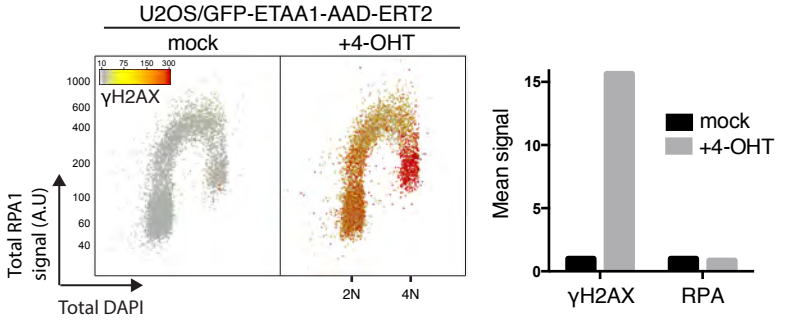

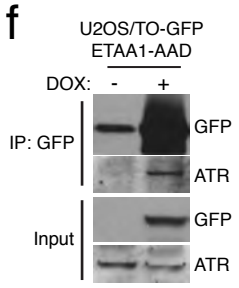

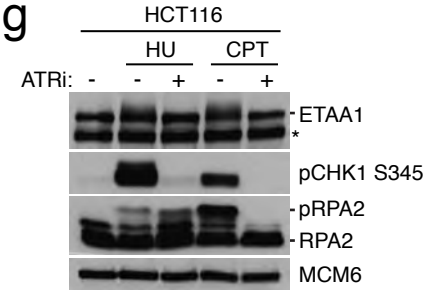

h

	Label	ATRi	4-OHT	ETAA1-AAD
EXP1	L	-	+	Nuclear
	H	-	-	Cytoplasmic
EXP2	L	-	+	Nuclear
	H	+	+	Nuclear

4 Biological Replicates each

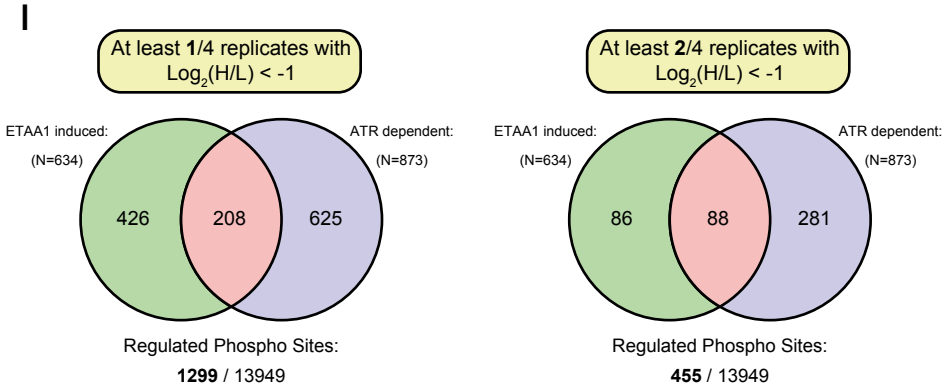

Haahr et al. Figure S4

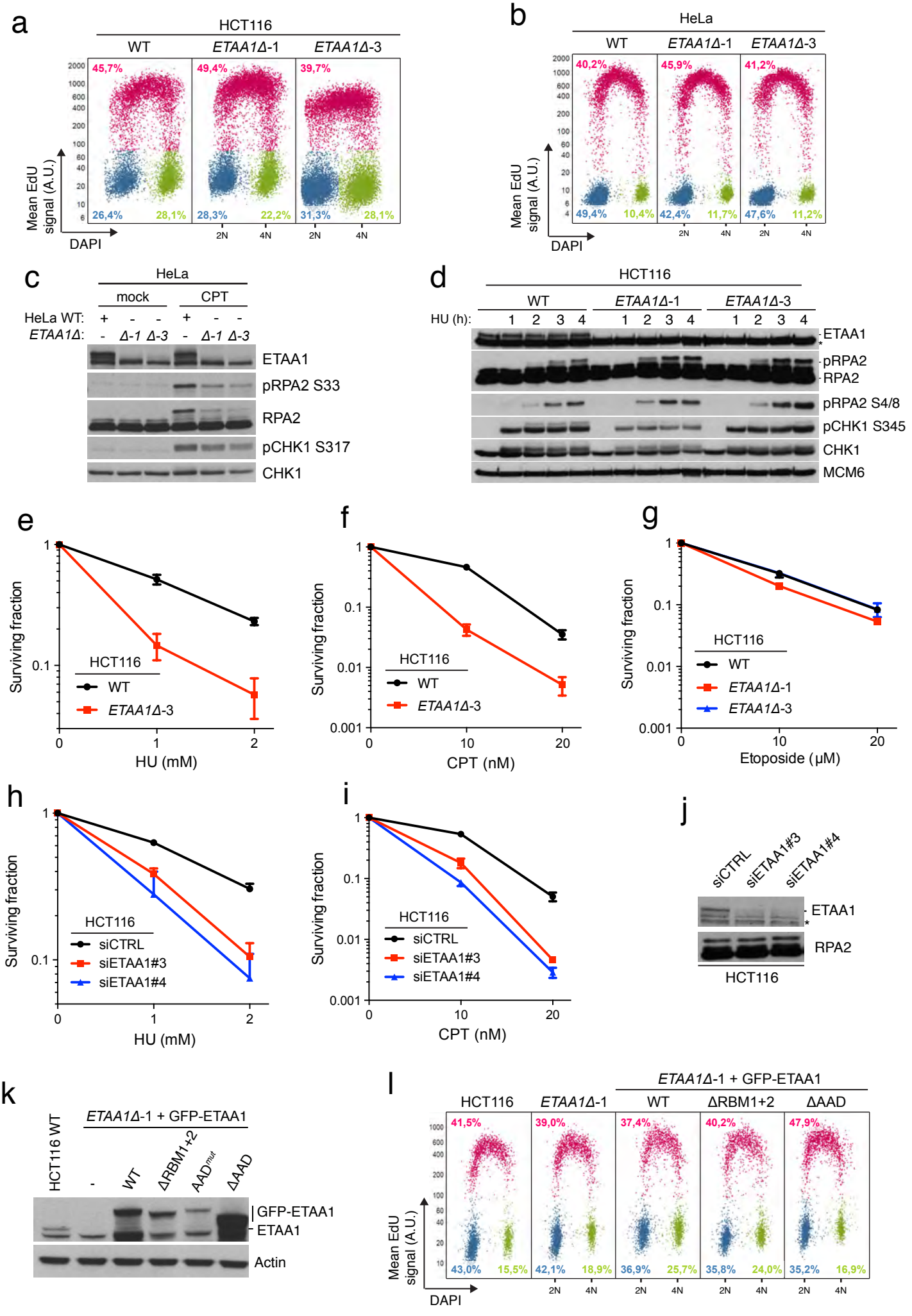

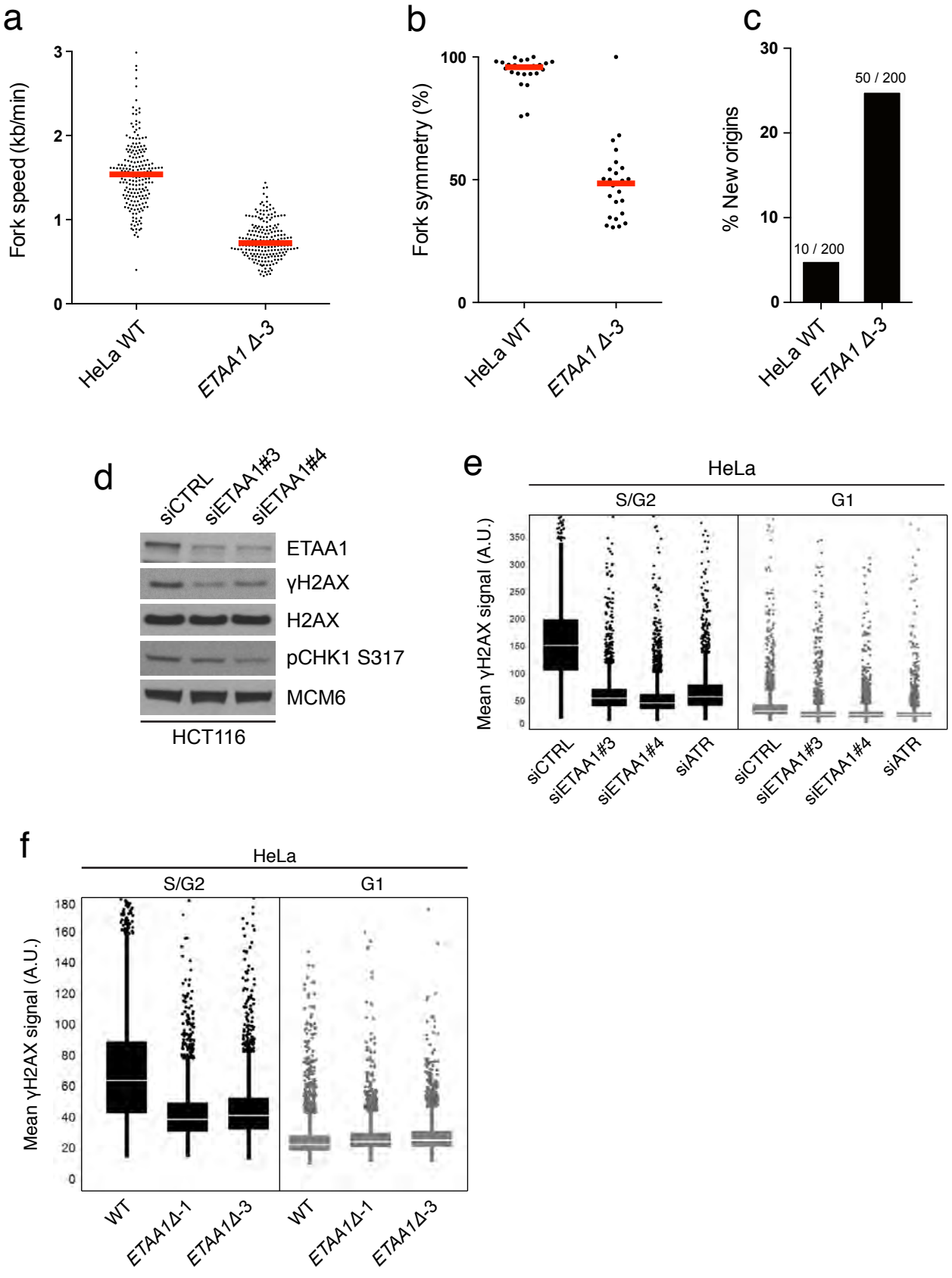
a
Fork speed (kb/min)
3
2
1
0
HeLa WT
ETAA1 Δ-3
b
Fork symmetry (%)
100
50
0
HeLa WT
ETAA1 Δ-3
c
% New origins
30
20
10
0
10 / 200
50 / 200
HeLa WT
ETAA1 Δ-3
d
siCTRL
siETAA1#3
siETAA1#4
ETAA1
γH2AX
H2AX
pCHK1 S317
MCM6
HCT116
e
HeLa
S/G2
G1
Mean γH2AX signal (A.U.)
350
300
250
200
150
100
50
0
siCTRL
siETAA1#3
siETAA1#4
siATR
siCTRL
siETAA1#3
siETAA1#4
siATR
f
HeLa
S/G2
G1
Mean γH2AX signal (A.U.)
180
160
140
120
100
80
60
40
20
0
WT
ETAA1Δ-1
ETAA1Δ-3
WT
ETAA1Δ-1
ETAA1Δ-3

Haahr et al. Figure S6

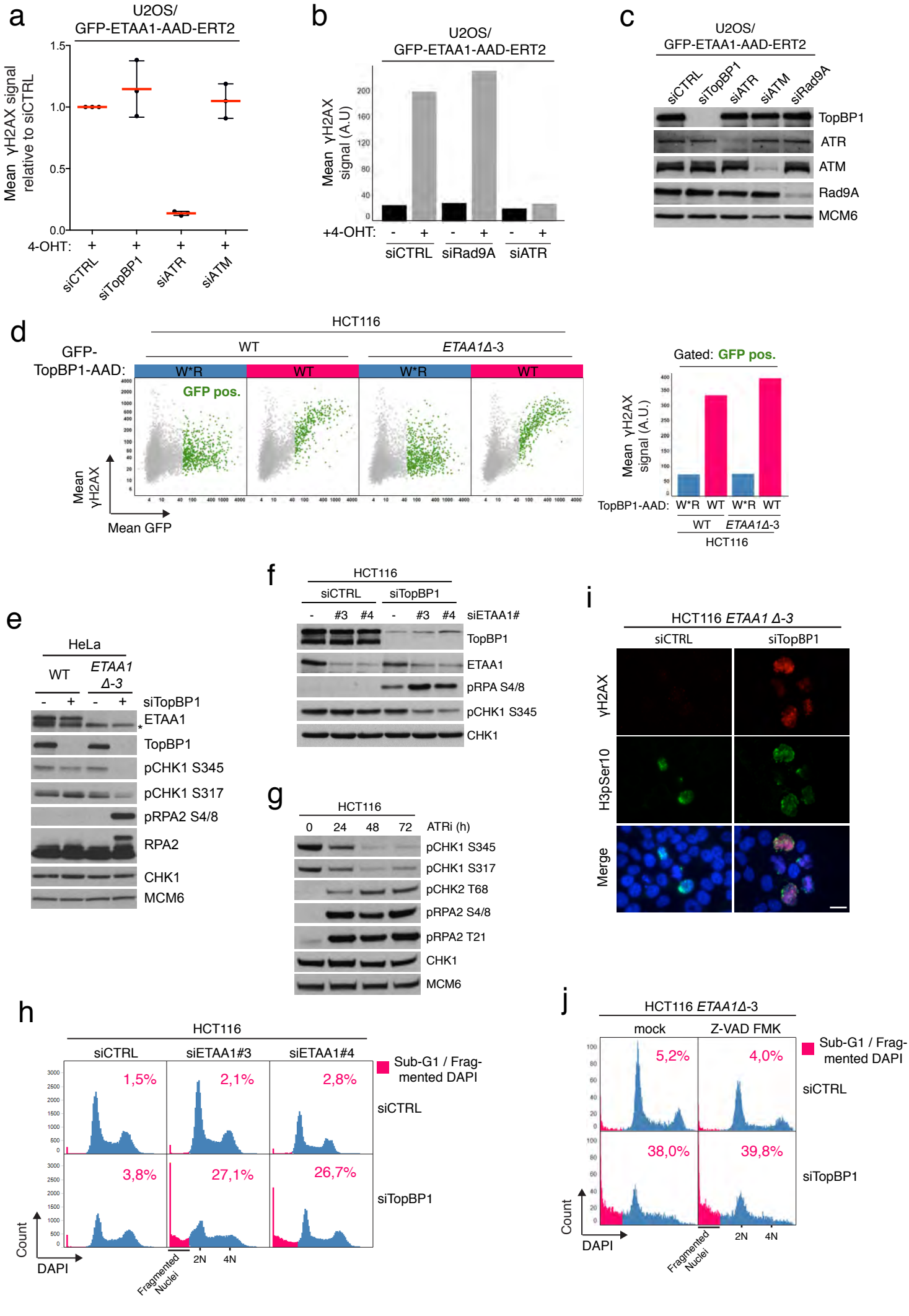

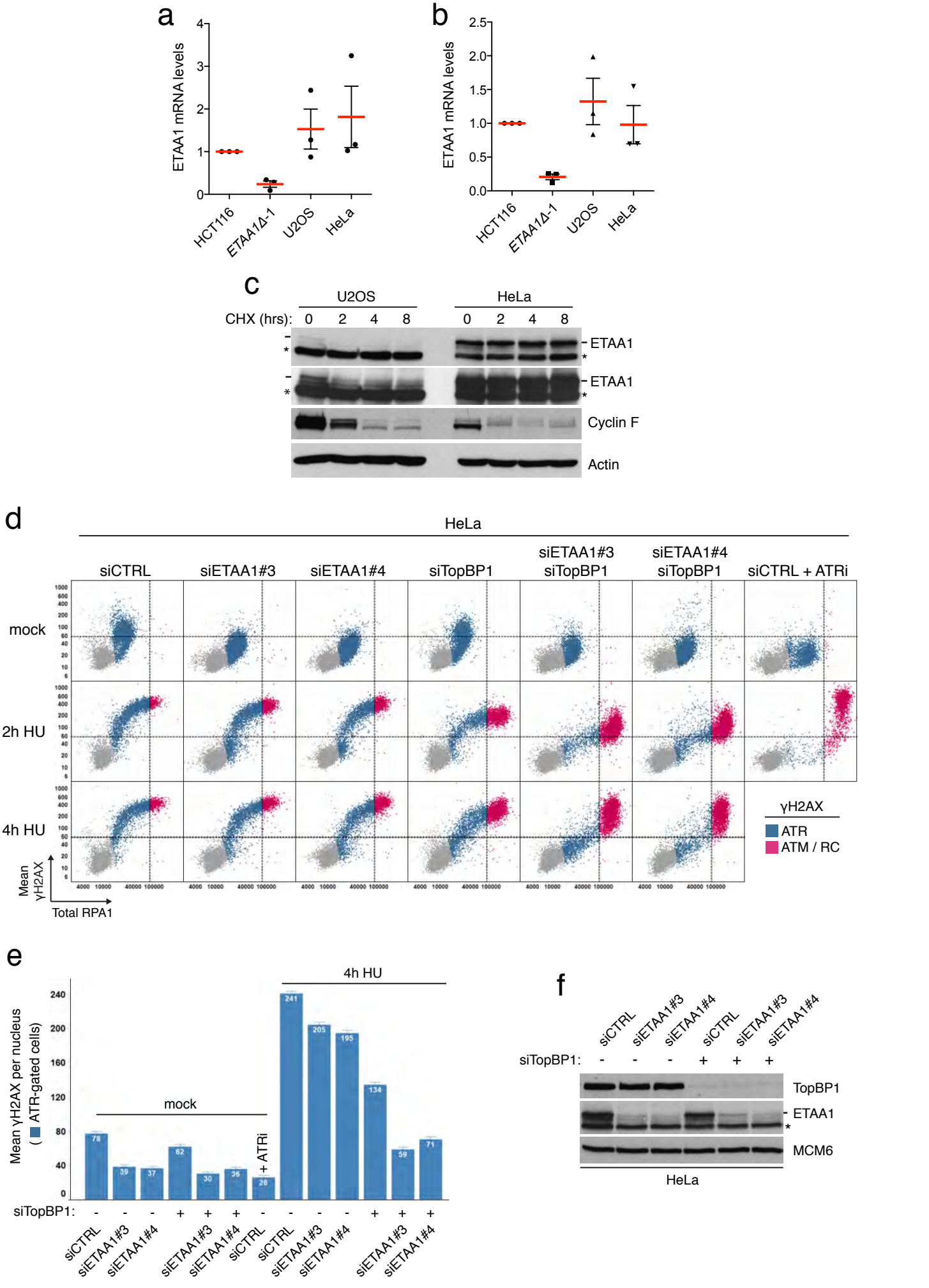
a
ETAA1 mRNA levels
HCT116
ETAA1Δ-1
U2OS
HeLa
b
ETAA1 mRNA levels
HCT116
ETAA1Δ-1
U2OS
HeLa
c
U2OS
HeLa
CHX (hrs): 0 2 4 8 0 2 4 8
ETAA1
ETAA1
Cyclin F
Actin
d
HeLa
siCTRL
siETAA1#3
siETAA1#4
siTopBP1
siETAA1#3 siTopBP1
siETAA1#4 siTopBP1
siCTRL + ATRi
mock
2h HU
4h HU
γH2AX
ATR
ATM / RC
Mean γH2AX
Total RPA1
e
4h HU
Mean γH2AX per nucleus (ATR-gated cells)
mock
+ ATRi
78
39
37
62
30
36
26
241
205
195
134
59
71
siTopBP1: - - - + + + - - - - + + +
siCTRL
siETAA1#3
siETAA1#4
siETAA1#3
siETAA1#4
siCTRL
siCTRL
siETAA1#3
siETAA1#4
siETAA1#3
siETAA1#4
f
siCTRL
siETAA1#3
siETAA1#4
siCTRL
siETAA1#3
siETAA1#4
siTopBP1: - - - + + +
TopBP1
ETAA1
MCM6
HeLa

Uncropped scans with size marker (kDa) indications

Figure 2a

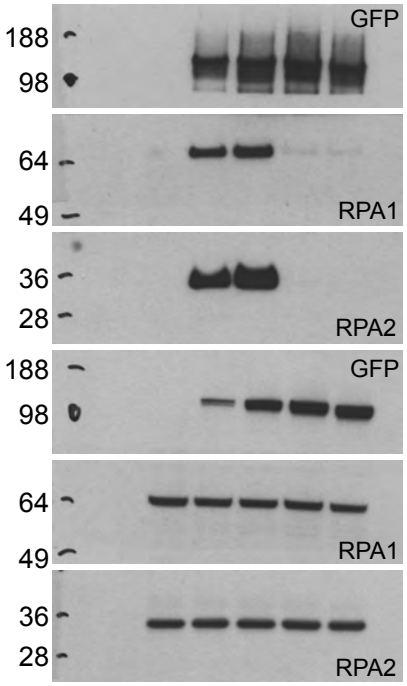

Figure 2c

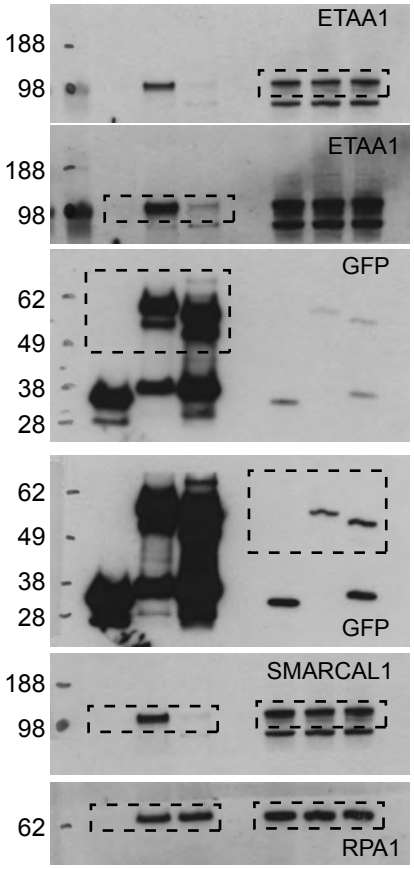

Figure 3g

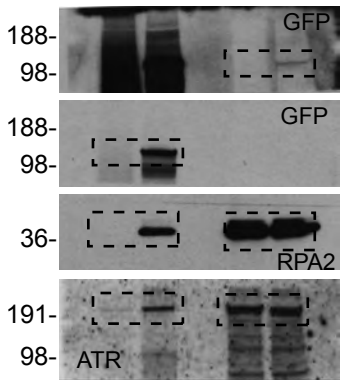

Figure 3j

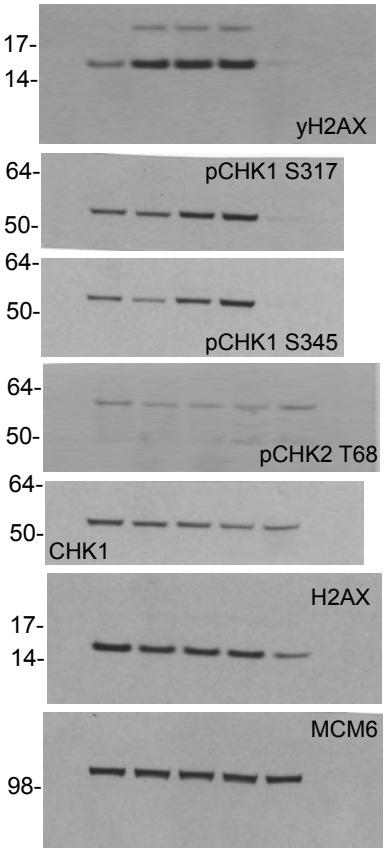

Figure 3h

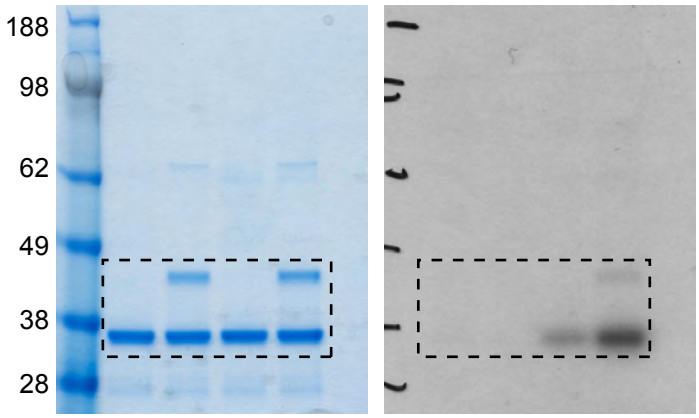

Figure 4a

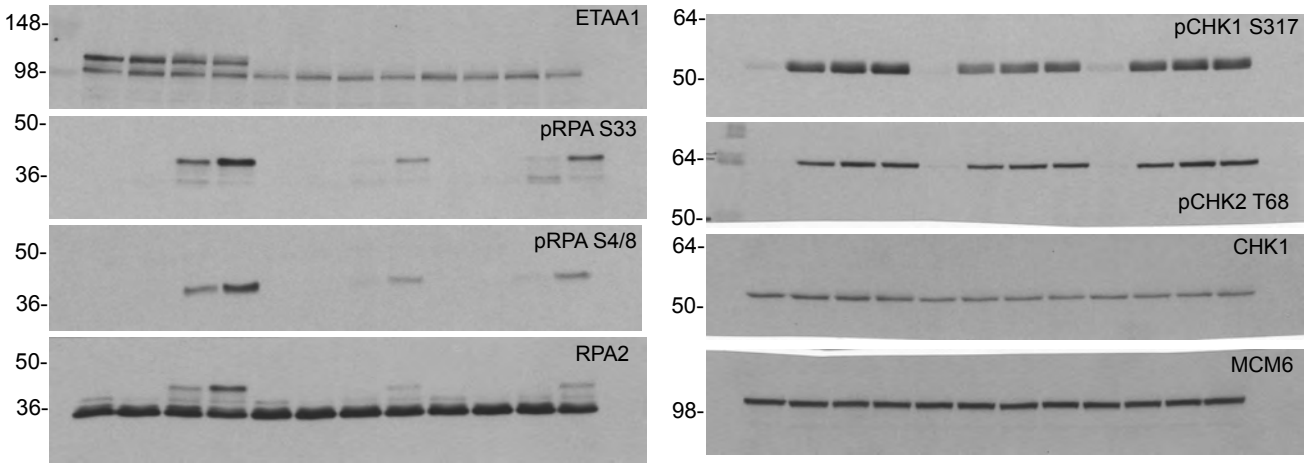

Figure 4b

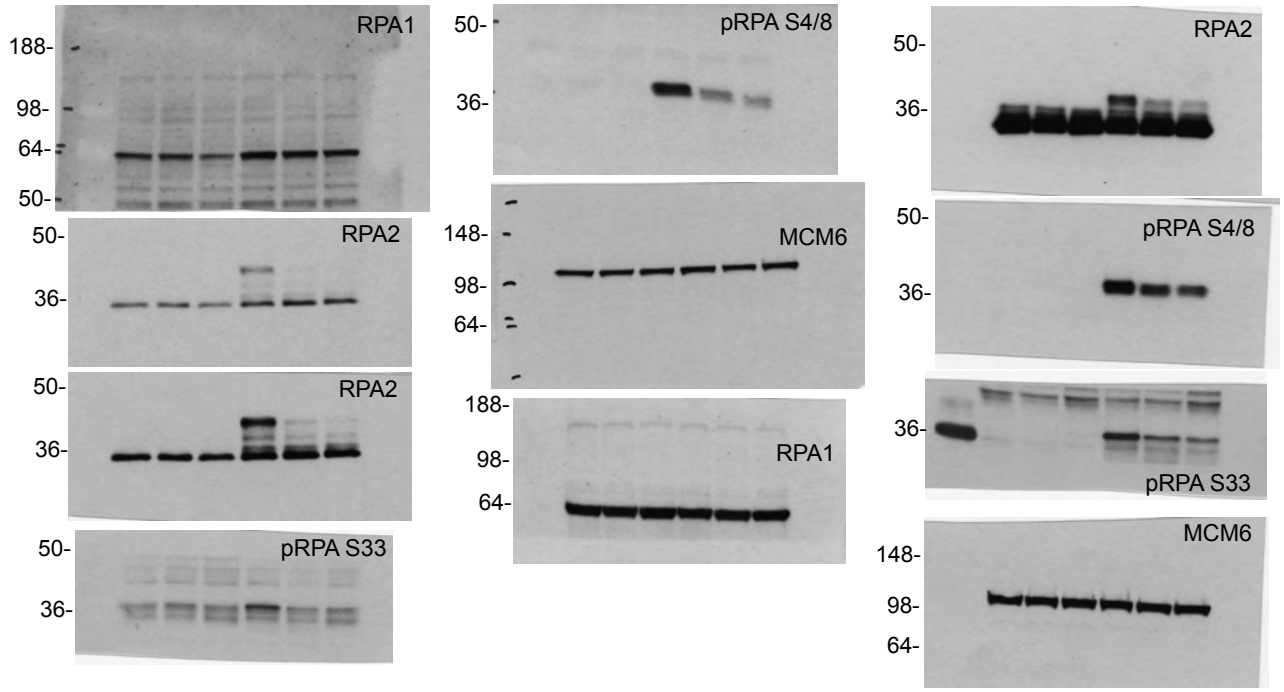

Figure 6b

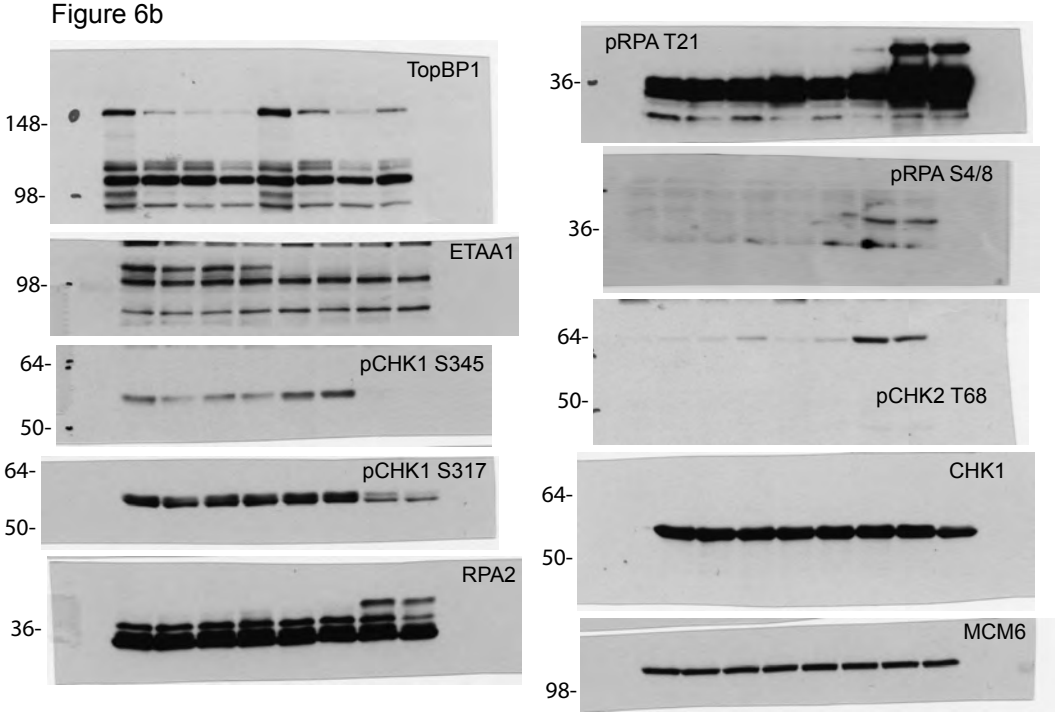

Figure 6g

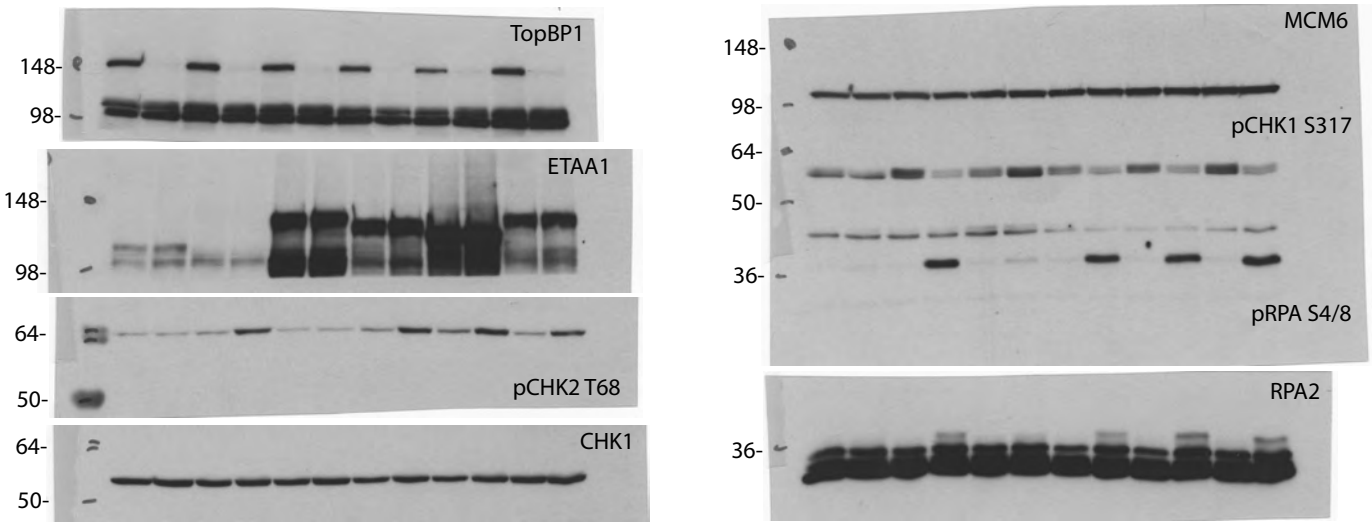

Figure 7a

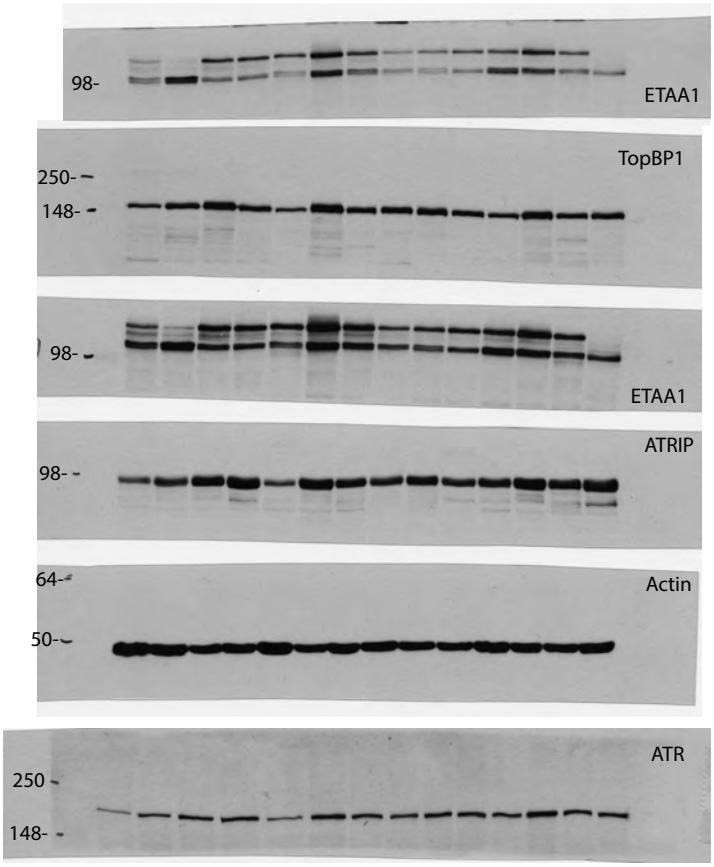

Figure 7b

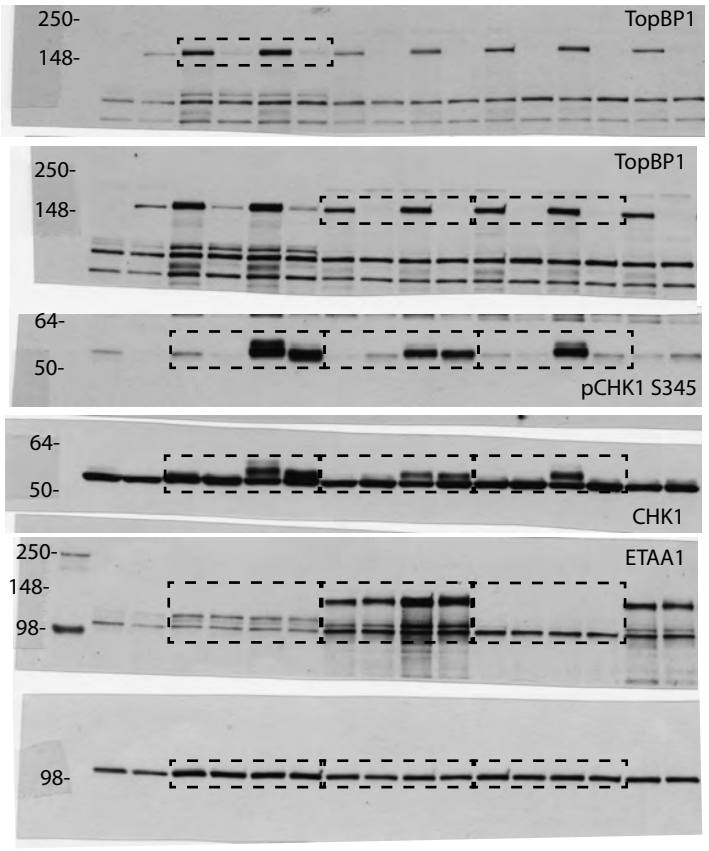

Figure S2a

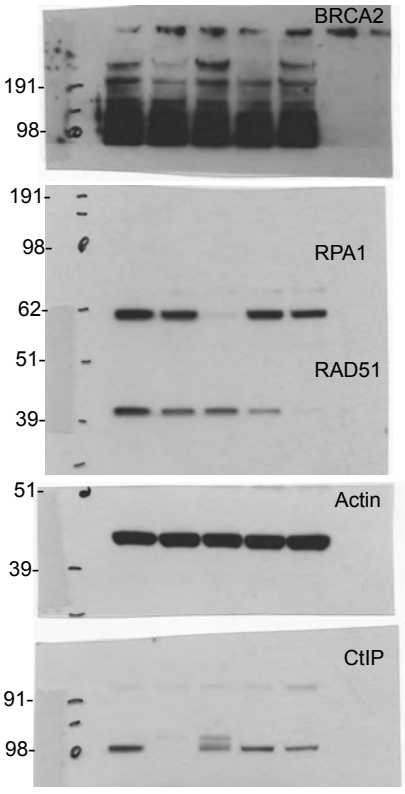

Figure S2e

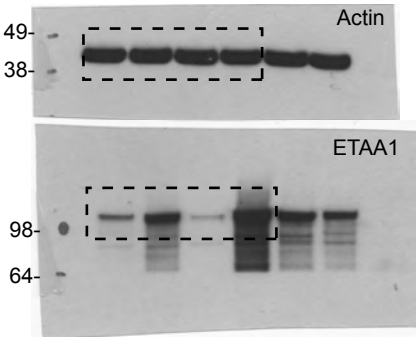

Figure S3g

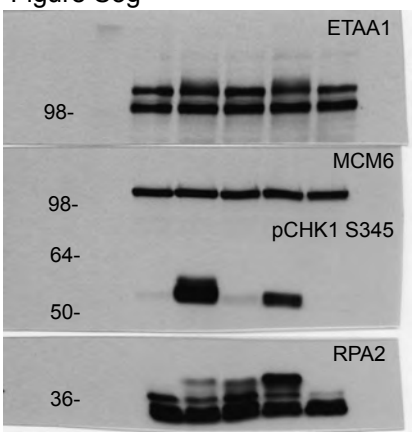

Figure S4c

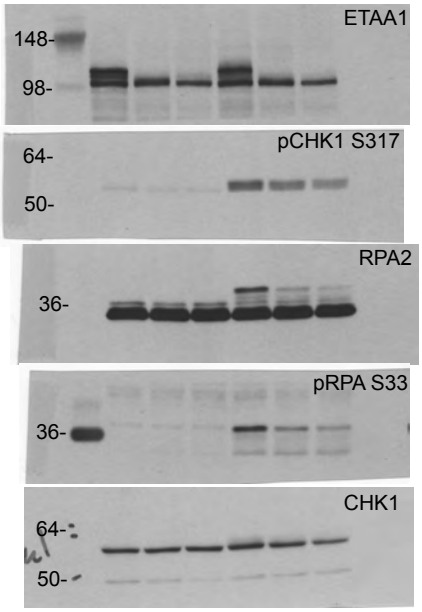

Figure S2b

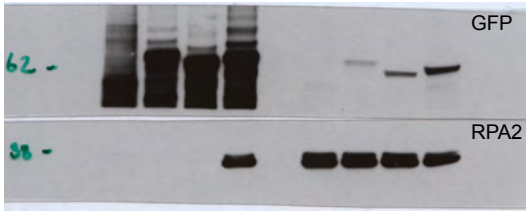

Figure S2f

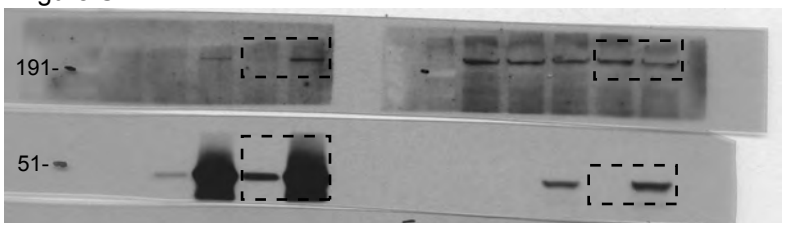

Figure S4d

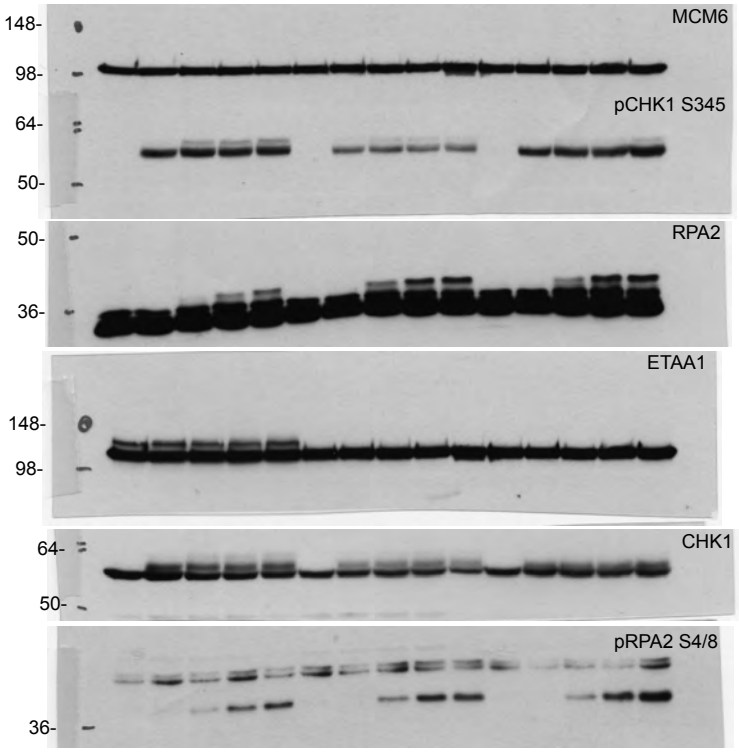

Figure S4i

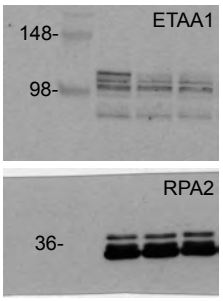

Figure S4k

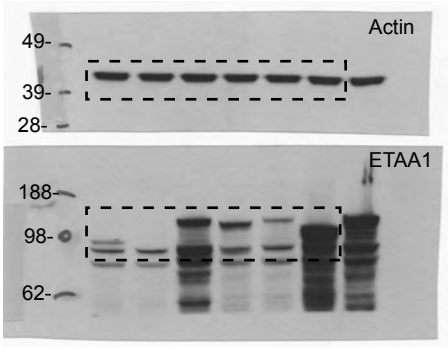

Figure S5d

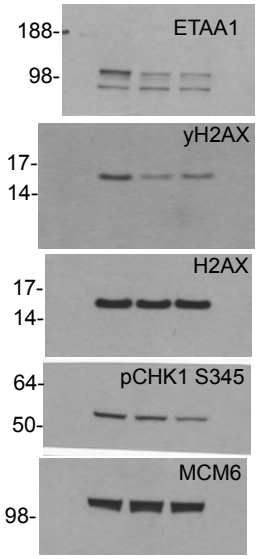

Figure S6c

Figure S6e

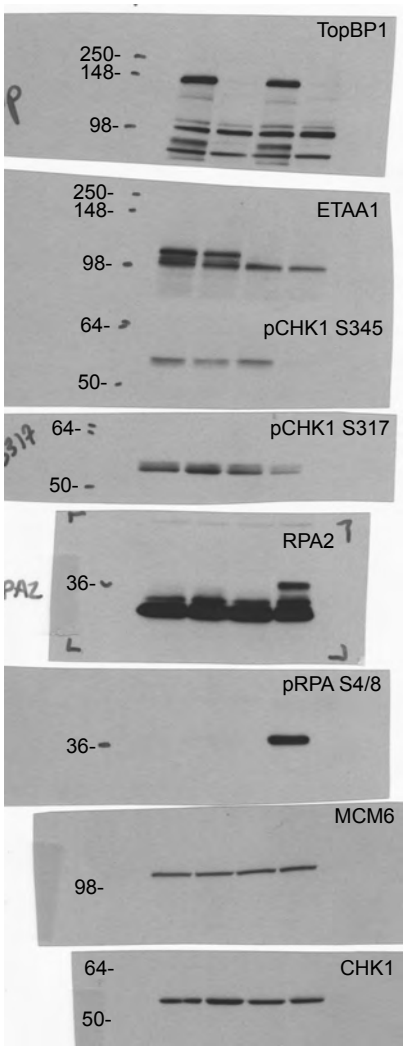

Figure S6f

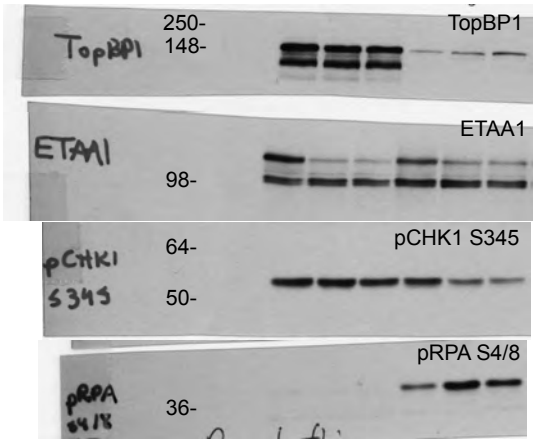

Figure S6g

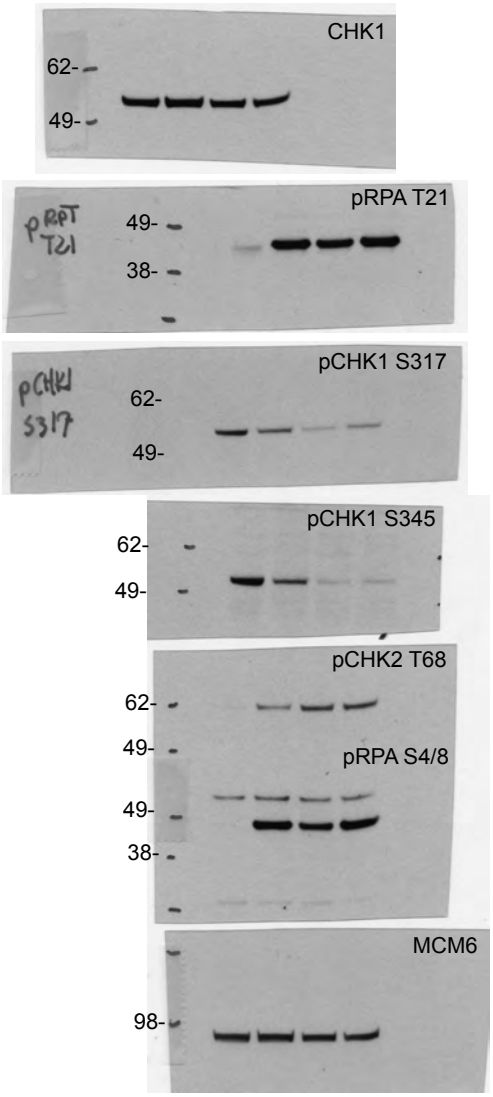

Figure S7c

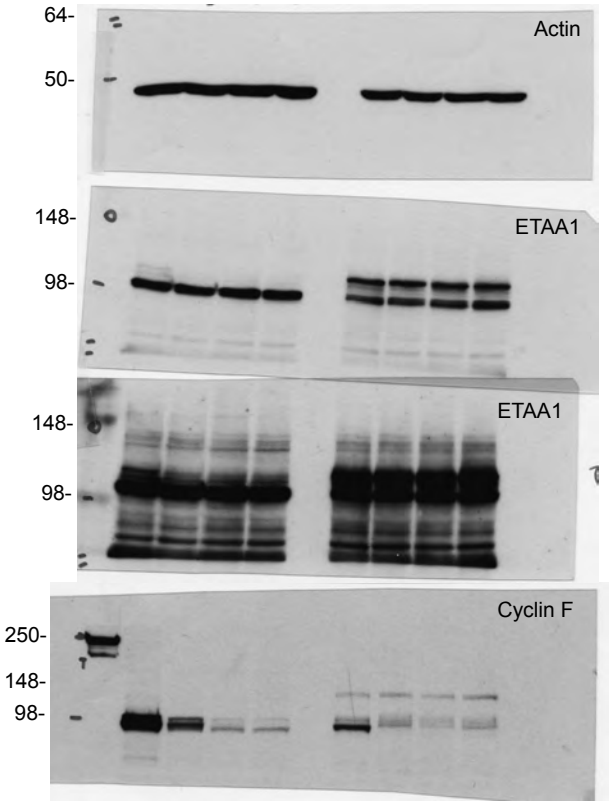

Figure S7f